

Deciphering age-related transcriptomic changes in the mouse retinal pigment epithelium

Sushil K. Dubey^{1,*}, Rashmi Dubey^{1,*}, Kyungsik Jung¹, Alvaro G Hernandez², Mark E. Kleinman¹

¹Department of Surgery, East Tennessee State University, Johnson City, TN 37614, USA

²Roy J. Carver Biotechnology Center, University of Illinois at Urbana-Champaign, Urbana, IL 61801, USA

*Equal contribution

Correspondence to: Mark E. Kleinman; email: kleinman@etsu.edu

Keywords: transcriptome, retinal pigment epithelium, oxidative stress, inflammation, chronological aging

Received: May 20, 2024

Accepted: February 18, 2025

Published: March 5, 2025

Copyright: © 2025 Dubey et al. This is an open access article distributed under the terms of the [Creative Commons Attribution License](https://creativecommons.org/licenses/by/4.0/) (CC BY 4.0), which permits unrestricted use, distribution, and reproduction in any medium, provided the original author and source are credited.

ABSTRACT

Aging of the retinal pigment epithelium (RPE) leads to a gradual decline in RPE homeostasis over time, significantly impacting retinal health. Understanding the mechanisms underlying RPE aging is crucial for elucidating the background in which many age-related retinal pathologies develop. In this study, we compared the transcriptomes of young and aged mouse RPE and observed a marked upregulation of immunogenic, proinflammatory, and oxidative stress genes in aging RPE. Additionally, aging RPE exhibited dysregulation of pathways associated with visual perception and extracellular matrix production. Research on aging in post-natal quiescent RPE is hindered by the absence of relevant *in vitro* models. Here, we evaluated an *in vitro* model of chronologically aged primary human RPE to address this gap and observed gene expression patterns comparable to native-aged RPE. Gene expression profiling in this model highlighted its potential utility in investigating cellular and molecular mechanisms of RPE aging and in screening of therapeutic compounds. In conclusion, our findings underscore the pivotal role of inflammation, immune activation, and oxidative stress in the aging RPE landscape and provide insights into why age increases the risk of retinal pathologies.

INTRODUCTION

The retinal pigment epithelium (RPE) is a monolayer of highly polarized cells positioned between the neuroretinal photoreceptors and the choroidal capillaries [1]. Originating from neuroectoderm, these post-mitotic cells display highly convoluted basal infoldings that attach to a specialized Bruch's basement membrane which is an acellular layer separating the RPE from the choriocapillaris. The RPE forms a critical physiologic barrier in the outer retina offering multifunctional support to the photoreceptor layer and facilitating essential visual cycle metabolism [1, 2]. The RPE plays a vital role in retinal homeostasis by maintaining the integrity of the outer-retina blood barrier and facilitating nutrient and oxygen diffusion from blood to photoreceptors. A core function of the RPE entails the processing of visual cycle intermediates with the

continuous exchange of retinal chromophores between photoreceptors and the RPE during which the RPE re-isomerizes all-trans-retinal to 11-cis-retinal and transports it back to photoreceptors [3, 4]. This process is central to the visual cycle and sustains photoreceptor function. Furthermore, the RPE stabilizes ion composition in the subretinal space through voltage-dependent ion conductance in its apical membrane which is also essential for maintaining photoreceptor excitability and viability [5]. Another critical role of the RPE is the phagocytosis of shed photoreceptor outer segments wherein the outer segments are digested and essential substances such as retinaldehyde are recycled and returned to photoreceptors to replenish light-sensitive outer segments [6]. Therefore, any damage and dysfunction in the RPE deleteriously affect the health of photoreceptors, degrade retinal function, and ultimately lead to vision loss.

During the physiological aging process, retinal tissues undergo functional decline and degeneration with the RPE serving as the primary site of damage in many age-related retinal diseases [7]. While aging itself may not invariably lead to the onset of conditions such as age-related macular degeneration (AMD), retinitis pigmentosa (RP), and diabetic retinopathy (DR), age-related changes can predispose the eye to these diseases [8]. AMD, a leading cause of vision loss in developed countries, is characterized by progressive degeneration of the RPE, retina, and choriocapillaris [9, 10]. Numerous studies have documented age-related physiological changes in the RPE and the underlying Bruch's membrane, including the accumulation of intracellular granules containing oxidized lipids known as lipofuscin, mitochondrial DNA damage, lysosomal dysfunction, buildup of metabolic debris, and drusen biogenesis which is a hallmark feature of AMD progression [11–14]. Drusen accumulation impedes diffusion from the choroidal circulation to the retina exerting adverse effects on both RPE and photoreceptors. Drusen has a complex composition that comprises many inflammatory proteins, including complement factors, cytokines, C-reactive protein, IgG, and major histocompatibility class II molecules [15, 16]. Elevated expression and localization of proinflammatory factors associated with drusen biogenesis trigger oxidative stress and cellular dysfunction, which have long been recognized as significant factors influencing the pathophysiology of AMD [12, 17]. Due to the neural retina's high energy requirements, the RPE remains metabolically active, constantly producing energy to support both the neural retina and the visual cycle. As a result, the RPE is abundant in mitochondria, making it a primary source of reactive oxygen species (ROS), and these mitochondria increase their ROS production during aging [18]. Despite scientific advancements that have established a multitude of molecular pathways significant in the pathogenesis of RPE atrophy and age-related retinal diseases, the genes driving biologic aging remain poorly understood [19, 20]. Deciphering differential gene expression profiles in young and aged RPE is critical to identifying molecular mechanisms that provide fundamental scientific insight into RPE aging and potential therapeutic targets for age-related retinal pathologies.

Chronological aging models of laboratory animals provide an extremely powerful experimental approach to studying molecular mechanisms that contribute to the development of age-related retinal diseases. Utilizing transcriptome-wide RNA sequencing, we studied differential gene expression profiles in the RPE/choroid of young and aged mice and identified global transcriptomic changes underlying the biologic aging of

the RPE. The molecular pathways significantly enhanced in aged RPE suggest a predisposition in older mice towards inflammation, immune activation, and oxidative stress, which are known drivers of age-related retinal pathologies. In a correlated *in vitro* model of primary human RPE isolates, chronological aging similarly resulted in gene expression profiles associated with increased inflammatory and oxidative stress responses. These findings significantly expand our fundamental scientific understanding of age-related retinal diseases while offering potential new biomarkers for clinical diagnosis and therapeutic strategies to reverse biologic aging in the RPE.

RESULTS

Transcriptome profiling of young and aged mouse RPE/choroid

RNA-seq data were generated from RPE/choroid tissues of both young (2–3 months) and aged (20–24 months) C57BL/6J mice ($n = 4$, two males and two females per group). This comprehensive approach aimed to capture the entire transcriptome profile and provide insights into age-related changes in gene expression in RPE/choroid. The sequencing depth averaged 50.2 million reads per library, with 21,376 transcripts mapped to the mouse reference genome (GRCm39). Of the 21,376 transcripts mapped, 73.92% were protein-coding, and 18.4% were assigned to long non-coding transcript types, making them the predominant transcript types (Figure 1A). The remaining ~3.8% represent other transcript types such as snoRNAs, miRNAs, snRNAs, unclassified ncRNAs, antisense lncRNAs, tRNA, rRNA, pseudogenes, and polymorphic pseudogenes (Figure 1A). Principal component analysis (PCA) was performed using the normalized read counts to obtain a global characterization of the mouse transcriptome. PCA revealed distinct clustering of young and aged groups along PC1, accounting for 52.4% of the variance, suggesting age as the primary driving factor (Figure 1B). To elucidate the biological processes underlying this segregation, Gene Ontology (GO) analysis was performed on the top 100 loading genes of PC1. Genes with positive loadings in PC1 exhibited enrichment in GO terms related to defense response, immune response, and inflammatory response pathways (Figure 1C), while genes with negative loadings in PC1 were enriched for GO terms associated with visual perception and phototransduction (Figure 1D and Supplementary Table 1).

Differential expression analysis using edgeR identified significant alterations in 5,469 genes between young and aged RPE/choroid samples (adjusted p -value < 0.05). The gene expression distribution across the

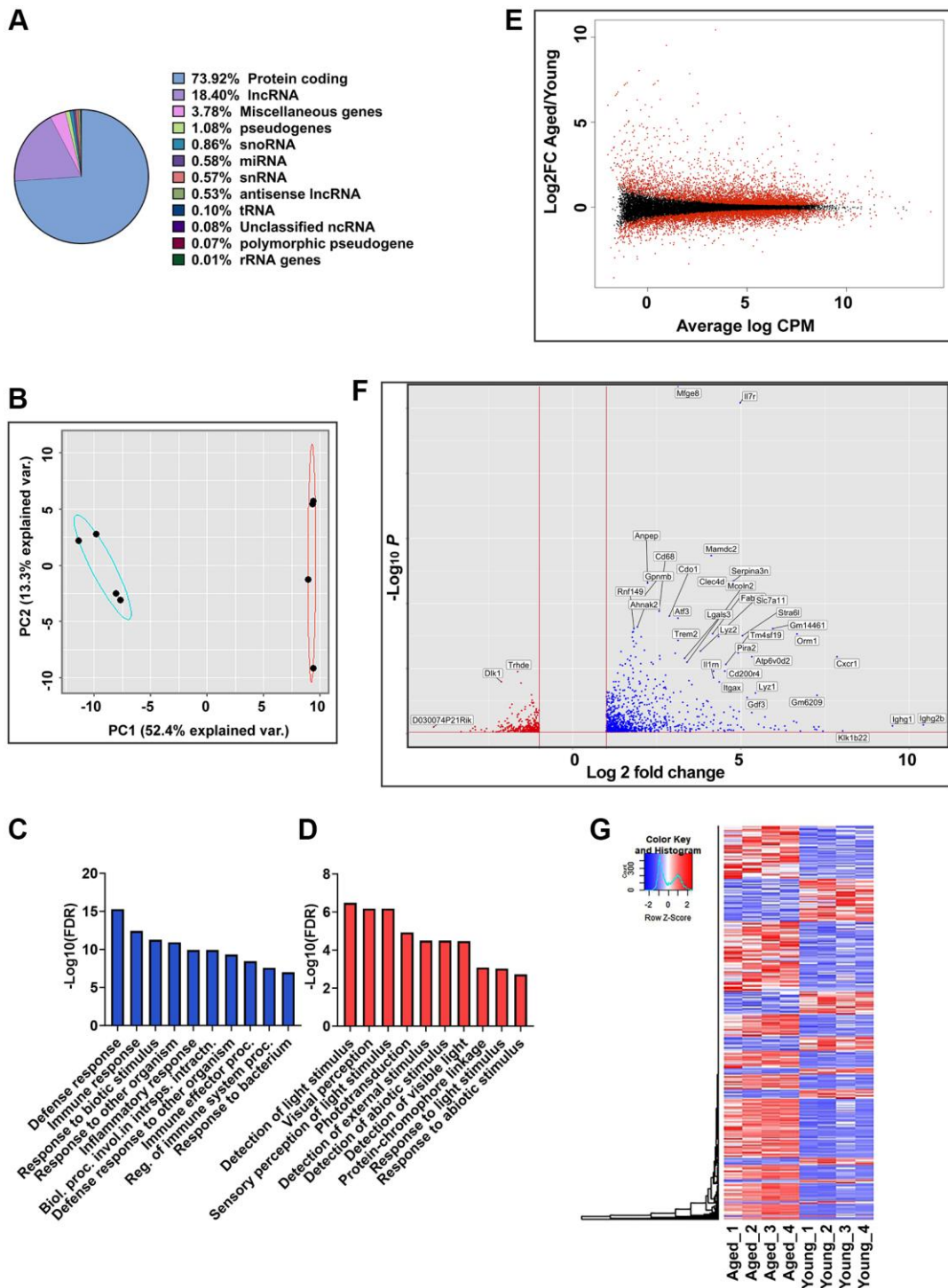


Figure 1. Global gene expression analysis in RPE/choroid of young and aged mice. (A) Pie chart represents the percent of globally expressed transcript subspecies across young (2–3 months, $n = 4$) and aged (22–24 months, $n = 4$) mice RPE/choroid from 21,376 annotated transcripts. (B) PCA plots of whole transcriptome data showed distinct clustering of young and aged mice along PC1, which captures the maximum variance (52.4%). Blue and red ellipses indicate young and aged mice and black dots represent the biological replicates ($n = 4$). (C, D) GO enrichment terms associated with the top 100 PC1 positive loading genes (C) and PC1 negative loading genes (D). (E) MA plot of log2 fold change versus average log counts-per-million (CPM) based on edgeR analysis showing the differential gene expression between aged and young mice RPE/choroid. Red dots indicate differentially expressed genes ($FDR \leq 0.05$), and black dots indicate non-differentially expressed genes. (F) Volcano plot showing genes significantly (p -adj value < 0.05) upregulated (red) and downregulated (blue) in aged mice RPE/choroid. The x-axis represents log2-fold change, and the y-axis represents $-\log_{10}$ (p -value). The dotted line shows a cutoff of $-\log_{10}$ (p -value) < 0.05 . Annotated dots represent the top significantly regulated genes. (G) Hierarchical clustering and heatmap analysis of gene expression in the RPE/choroid tissues of the young vs. aged mice. Blue to red represents low to high gene expression.

entire transcriptome dataset was depicted through an MA plot (Figure 1E). Thresholds of the adjusted p -value < 0.05 and \log_2 fold change (Log_2FC) ≤ -1 and $\geq +1$ were applied to define differentially expressed genes (DEGs). Analysis revealed 1,300 DEGs, including 939 upregulated and 361 downregulated genes in aged RPE compared to young RPE. A volcano plot illustrated the magnitude of differential expression (Figure 1F) with higher transcriptional activation in aging mouse RPE/choroid, as measured by both the number of DEGs induced and their Log_2FC s. Furthermore, hierarchical clustering and heatmap analyses of these DEGs illustrated distinct expression profiles between young and aged groups consistent with age-associated alterations in RPE gene expression (Figure 1G).

Gene enrichment analysis reveals induction of immune and inflammatory response in aged mouse RPE/choroid

To further elucidate the characteristics of the DEGs, we performed a GO analysis using the top 100 significantly upregulated and downregulated genes. The functional GO terms were classified into three categories: biological process (BP), cellular component (CC), and molecular function (MF), as shown in Figure 2A, 2B. For genes upregulated in aged RPE, GO analysis revealed a notable enrichment in biological processes associated with immune response, regulation of immune system processes, inflammatory response, defense response, cell activation, positive regulation of immune system processes, regulation of immune response, leukocyte activation, immune effector processes, and leukocyte-mediated immunity. Additionally, molecular function and cellular component GO terms displayed enrichment in signaling, receptor activity, extracellular space, and cell surface, indicative of active proinflammatory milieu in the aging RPE (Figure 2A and Supplementary Table 2). GO annotation of downregulated genes included processes related to visual perception, sensory perception of light stimulus, detection of light stimulus, detection of visible light, detection of external stimulus, detection of abiotic stimulus, phototransduction, cellular response to interferon-beta, response to interferon-beta, and response to light stimulus (Figure 2B). This decline in the expression of genes associated with visual pathways and phototransduction is consistent with the potential degeneration of RPE and impaired vision associated with aging. Photoreceptor outer segment and G-protein coupled photoreceptor activity were the most significantly enriched GO terms in the cellular component and molecular function categories, respectively (Figure 2B and Supplementary Table 2). These findings suggest that genes implicated in crucial RPE functions, such as maintaining visual processing in

the retina including absorption of light passing through the neurosensory retina, phagocytosis of photoreceptor outer segments, and sustaining the retinoid cycle or visual cycle are impacted by aging.

DEGs were then mapped to their biologically relevant pathways using the KEGG pathway database. Among the ten most significantly upregulated pathways in aging RPE, the majority were immune-related (Figure 2C) with the cytokine-cytokine receptor pathway being the most enriched (p -value: $7.4\text{E}-19$; Supplementary Figure 1). This finding aligns well with the results of the GO analysis, as cytokine production is known to be highly responsive to inflammation in the RPE [21]. Within this pathway, a total of 94 genes exhibited significant alterations in aged RPE/choroid comprising both receptor and ligand molecules including numerous chemokines, cytokines, interleukins, TNF, and TGF factors. This extensive modification underscores the presence of a robust autocrine and paracrine signaling milieu in aging RPE (Supplementary Figure 1). Other prominent age-related networks that emerged from KEGG analysis were osteoclast differentiation, complement activation, and coagulation cascades (Figure 2C). In contrast, downregulated genes did not exhibit significant enrichment in any pathways, potentially due to many of these genes lacking annotations in specific KEGG pathways. Therefore, we expanded our analysis to include 1,418 genes using a threshold of adjusted p -value < 0.05 and $\text{Log}_2\text{FC} \geq 0.5$ for KEGG analysis. Among the top three downregulated pathways were phototransduction, protein digestion and absorption, and extracellular matrix (ECM)-receptor interaction (Figure 2D). The downregulation of the phototransduction pathway and dysregulation of protein turnover emerged as key processes in aging RPE. Furthermore, the loss of ECM-receptor interaction underscores a hallmark of RPE aging which likely contributes to the disorganization of the ECM [22].

Establishment of PPI networks and hub gene analysis

We constructed a Protein-Protein Interaction (PPI) network utilizing the STRING database (v12.0) and Cytoscape software to evaluate the relationship among the upregulated DEGs in the aging RPE [23]. To ensure the reliability of the PPIs, we set a stringent cutoff threshold of a high confidence interaction score of ≥ 0.9 , resulting in a robust PPI network comprising 726 nodes and 437 edges. Using the Cytoscape MCL mode, DEGs were subclustered within the PPI network, with the top five significant KEGG pathways assigned to distinct clusters (Figure 3A). Subsequently, interactions within the network were leveraged to identify hub genes using the Maximal Clique Centrality (MCC) algorithm in the

CytoHubba plugin [24] of Cytoscape. In this analysis, genes with the top 20 MCC scores were designated as hub genes (Figure 3B). Among these 20 hub genes were key players involved in the NADPH oxidase complex (*Cyba*,

Cybb, *Ncf1*, *Ncf2*, *Ncf4*, *Nox4*, *Rac2*), the complement pathway (*C1qa*, *C1qb*, *C1qc*, *C1ra*, *C1s1*, *C4b*, *Serping1*), and chemokines and chemokine receptors (*Ccl2*, *Cxcl1*, *Cxcl12*, *Cxcl5*, *Cxcr2*) (Figure 3B).

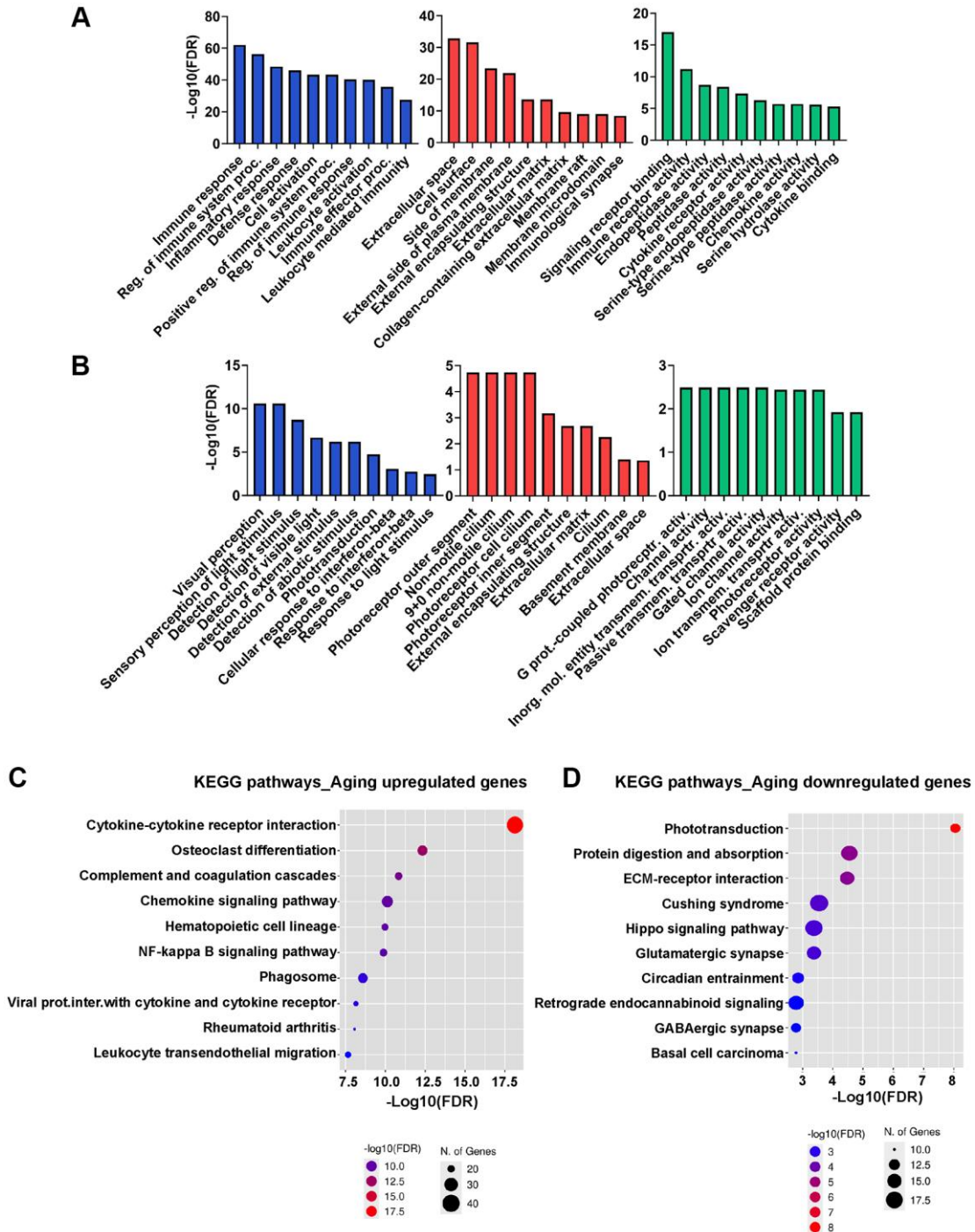


Figure 2. GO and KEGG functional enrichment analysis. (A, B) GO analysis of upregulated (A) and downregulated (B) genes in aged RPE/choroid in the BP, CC, and MF categories. The x-axis displays the top 10 most significant GO terms, and the y-axis represents the $-\log_{10}$ (FDR) of the enriched terms. (C, D) Dot plot showing KEGG pathway enrichment analysis of upregulated (C) and downregulated (D) genes in aged RPE/choroid. The y-axis presents the names of the top 10 enriched pathways, and the x-axis represents the $-\log_{10}$ (FDR). The number of DEGs enriched in a pathway is denoted by bubble size, and the $-\log_{10}$ (FDR) is reflected by the bubble's color. Abbreviations: DEGs: differentially expressed genes; GO: Gene Ontology; CC: cellular component; MF: molecular function; BP: biological process; KEGG: Kyoto Encyclopedia of Genes and Genomes.

A similar analysis was performed using the 1,418 DE genes (p -value < 0.05 and $\text{Log}_2\text{FC} \geq 0.5$) downregulated in aging RPE. These genes were integrated into a

coexpression network at a cutoff threshold of ≥ 0.9 confidence interaction score utilizing STRING and Cytoscape with 776 nodes and 181 edges. The DEGs

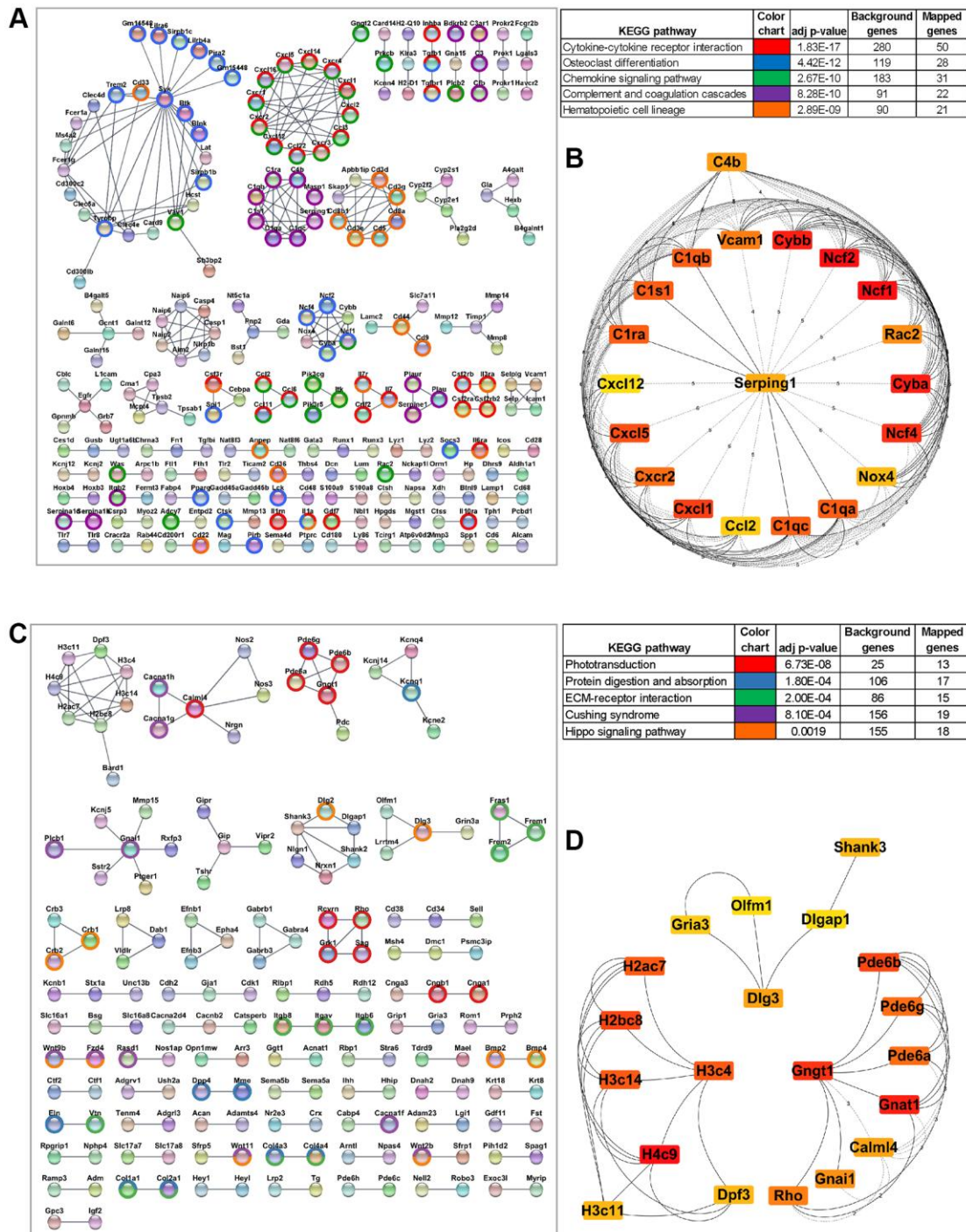


Figure 3. Protein-protein interaction (PPI) network of differentially expressed genes and the hub genes. (A) STRING network of PPI generated using DE genes upregulated in aging RPE/choroid (FDR < 0.05, log_2 fold change > 1). Significant clusters from the PPI network complex were constructed using the Cytoscape MCL plugin. Genes mapped to top KEGG pathways are highlighted. **(B)** The top 20 hub genes in the PPI network were identified using the Cytoscape plugin cytoHubba based on their maximal clique centrality (MCC) score. The 20 identified hub genes are displayed from red (high MCC score) to yellow (low MCC score). **(C)** PPI network constructed using DE genes downregulated in aging RPE/choroid (FDR < 0.05, log_2 -fold change > 0.05). The network is subclustered using the Cytoscape MCL plugin and the highlighted genes are mapped to top KEGG pathways. **(D)** Top 20 aging downregulated hub genes screened by the cytoHubba plugin of Cytoscape based on the MCC score where red nodes represent a higher MCC score and yellow represents a lower score.

were further subclustered using the Cytoscape MCL function and mapped to various KEGG pathways (Figure 3C). The most significant cluster, comprising 20 hub genes, was identified using the MCC algorithm (CytoHubba), consisting of genes central to chromatin organization (*H2ac7*, *H2bc8*, *H3c11*, *H3c14*, *H3c4*, *H4c9*, *Dpf3*), visual perception (*Pde6a*, *Pde6b*, *Pde6g*, *Gnat1*, *Calml4*, *Gnai1*, *Rho* and *Gngt1*), and neuronal synapse genes (*Shank3*, *Dlg3*, *Dlgap1*, *Olfml1*, *Gria3*) (Figure 3D).

Validation of RNA-seq profiles by qPCR

We validated our RNA-seq data findings through qPCR analysis using a new cohort of animals. We selected 31 genes: 12 age-upregulated, 17 age-downregulated, and two genes that showed no significant difference between young and aged RPE. The age-upregulated representative genes of major pathways included *Cybb*, *Cyba*, *Ncf1*, *Ncf2*, and *Ncf4* for the oxidative stress and redox pathway, *Clqb*, *C3*, *C4b*, and *C1s1* for the complement pathway, *Cxcr1* and *Cxcr4* for chemokine

response and *Best1*, an RPE-specific marker (Figure 4A). For transcripts downregulated in aging, we analyzed *Rpe65*, the classical RPE biomarker; histones *H1f0* and *H3c11*; hub genes *Gnai1*, *Gria3*, *Gnat1*; visual and phototransduction pathway genes *Opn1mw*, *Rdh8*, *Rbp3*, *Gpc3*, *Rdh12*, *Rdh5*, *Napepld*, *Bco2*, *Grk4*, *Gucy2f*, and the epigenetic regulator *Tet1* (Figure 4B). Additionally, we verified the expression of other epigenetic regulators, *Hdac3* and *Hdac8*, which remained unchanged with age (Figure 4B). The results of these expression analyses corroborated the RNA-seq data. In line with the RNA-seq and qPCR results, immunofluorescence (IF) staining of retinal cross sections in mice showed increased expression of C4b and reduced expression of H1f0 in aged mice RPE compared to young cohorts (Supplementary Figure 2).

Hub genes mapping and pathway visualization

We utilized the WikiPathways app within the Cytoscape network analysis and visualization software to conduct

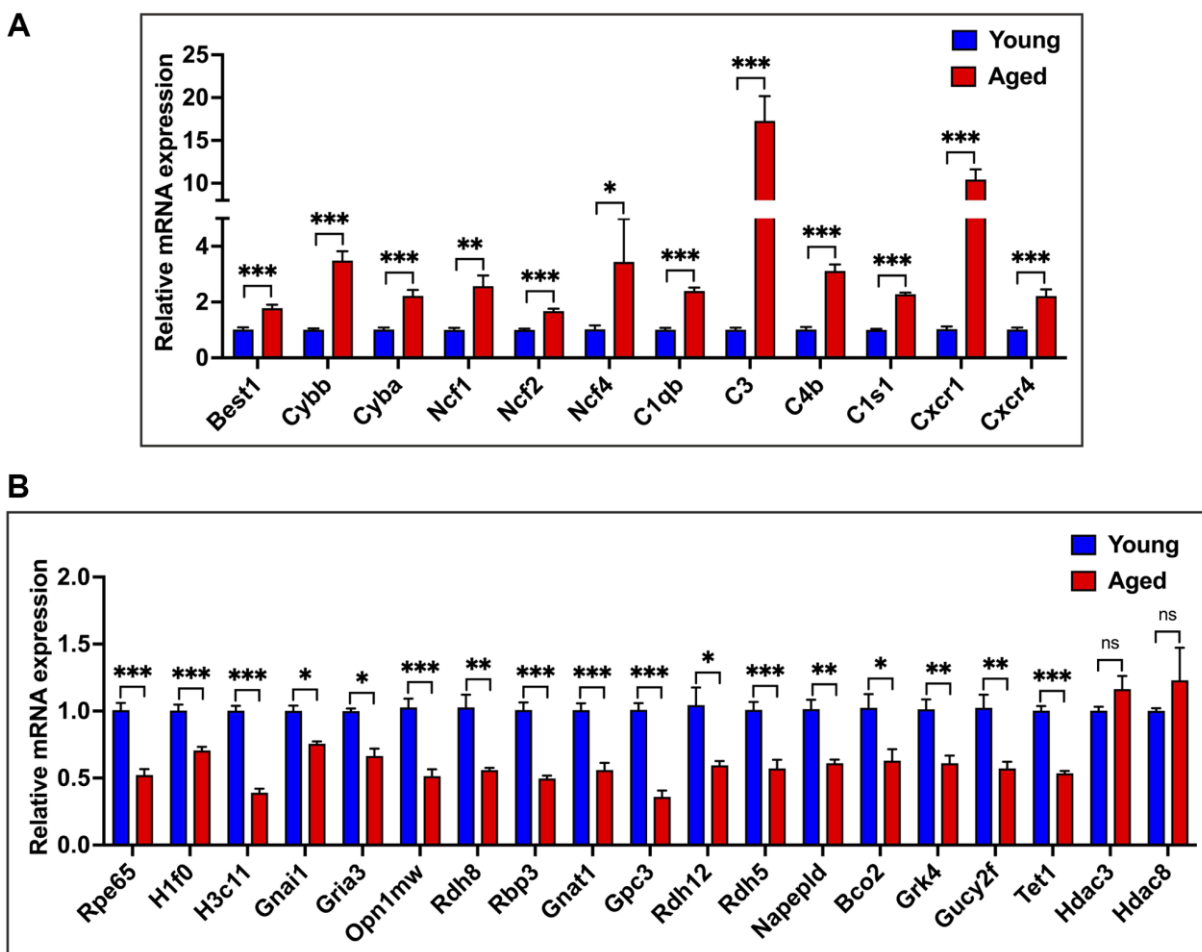


Figure 4. qPCR validation of RNA-seq data. (A) qPCR expression analysis of 12 genes upregulated in aged RPE/choroid. (B) Relative mRNA expression levels of genes downregulated in aging and not differentially regulated in RPE/choroid from young and aged mice. Actin-B was used for normalization, and statistical analysis was performed using the unpaired *t*-test (**p* < 0.05, ***p* < 0.01, ****p* < 0.001, ns: nonsignificant). Data were presented as mean ± SEM.

Moreover, several genes associated with these pivotal pathways were also significantly altered in our transcriptome dataset. The majority of these genes exhibited positive regulation, indicating the crucial involvement of oxidative stress, complement, and the chemokine system in RPE aging (Figure 5A, 5B and Supplementary Figure 1).

Age-related expression profiles of RPE signature genes

A comprehensive study by Bergen et al. compiled a list of 171 human RPE-specific markers [26]. We performed a comparative analysis between these RPE signature genes and our transcriptome data to identify age-related changes. Of these, 162 genes aligned with our dataset, revealing significant differential gene expression in 85 RPE marker genes between young and aged mice. The heatmap showed that a significant number of these genes were downregulated in aging RPE (Figure 6A). GO analysis indicated that 67 downregulated genes were involved in visual perception, sensory perception of light

stimulus, retinol metabolic process, morphogenesis of an epithelial bud, retinoid metabolic process, diterpenoid metabolic process, camera-type eye development, terpenoid metabolic process, transmembrane transport, and morphogenesis of an epithelial fold, consistent with declining functional ability and metabolic processes in the aged eye (Figure 6B). Among these 171 RPE-specific signature genes, 77 exhibited no significant changes in expression, and these included genes enriched in cytoskeleton organization and spindle organization (data not shown). Although these genes remained unchanged between young and aged RPE, they highlight the biological processes that remain unaltered with advancing age. Therefore, these genes are probably more robust RPE-specific markers in the context of aging and senescence.

Acquisition of inflammatory and immune active phenotypes by *in vitro* hRPE aging models

Next, we utilized long-term primary human RPE (hRPE) cultures ($n = 3$ isolates) to evaluate their

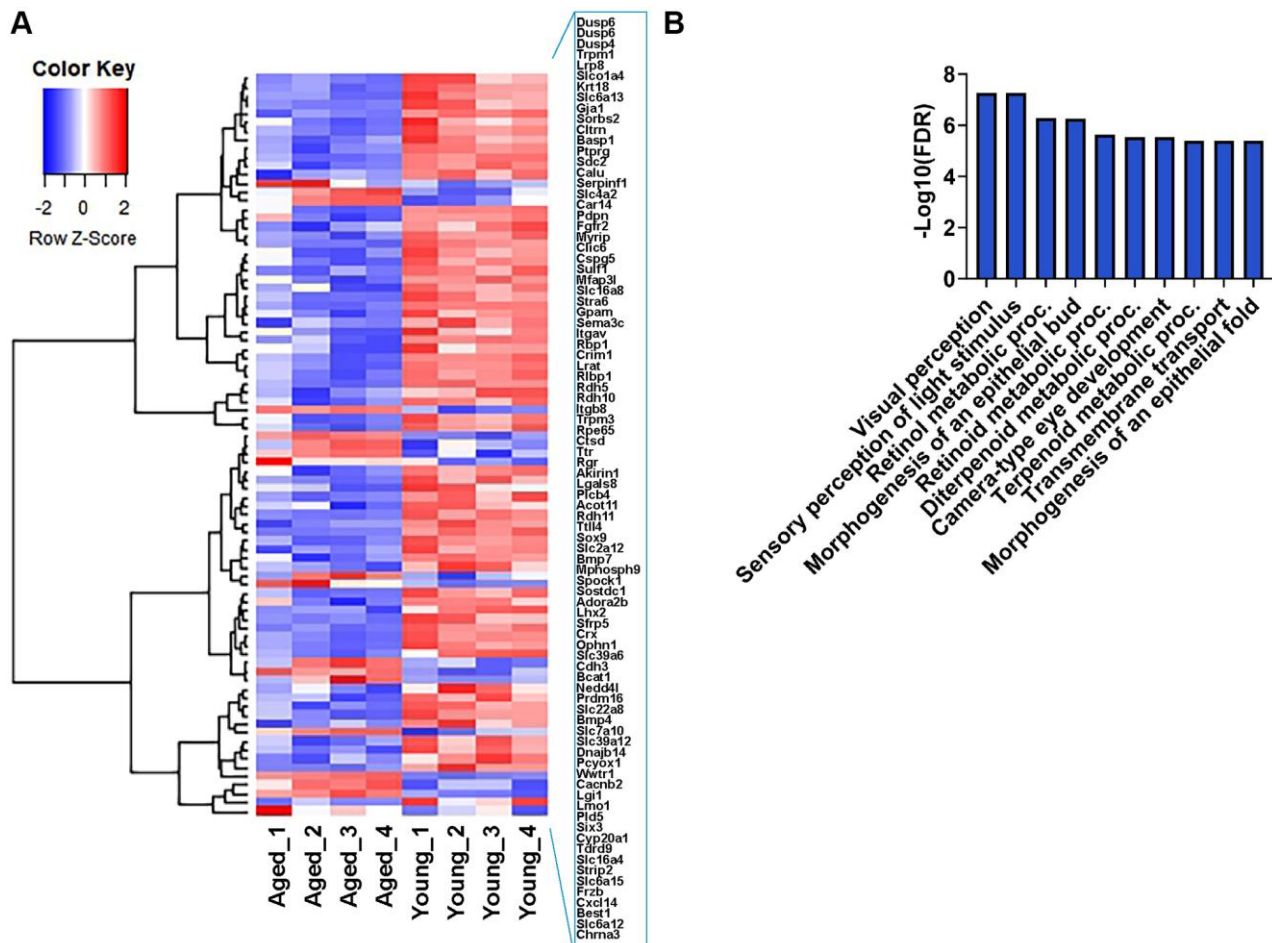


Figure 6. Expression profile of RPE-specific genes. (A) Hierarchical clustering and heatmap analysis of selected RPE-specific markers in the RPE/choroid of young and aged mice. Blue to red represents low to high gene expression. (B) GO term enrichment analysis of 67 RPE-specific genes that were downregulated in aging.

suitability as a model for studying RPE aging by comparing their characteristics with *in vivo* models. To establish *in vitro* aged RPE cultures from human donors, isolated RPE cells were cultured for up to 60 days according to the protocol outlined in the methods

section. By day 2, these long-term cultures exhibited 100% confluency and a hexagonal lattice morphology reminiscent of native RPE tissue *in vivo*. Long-term culture of hRPE developed dense pigmentation after approximately 21 days (Figure 7A). Confocal

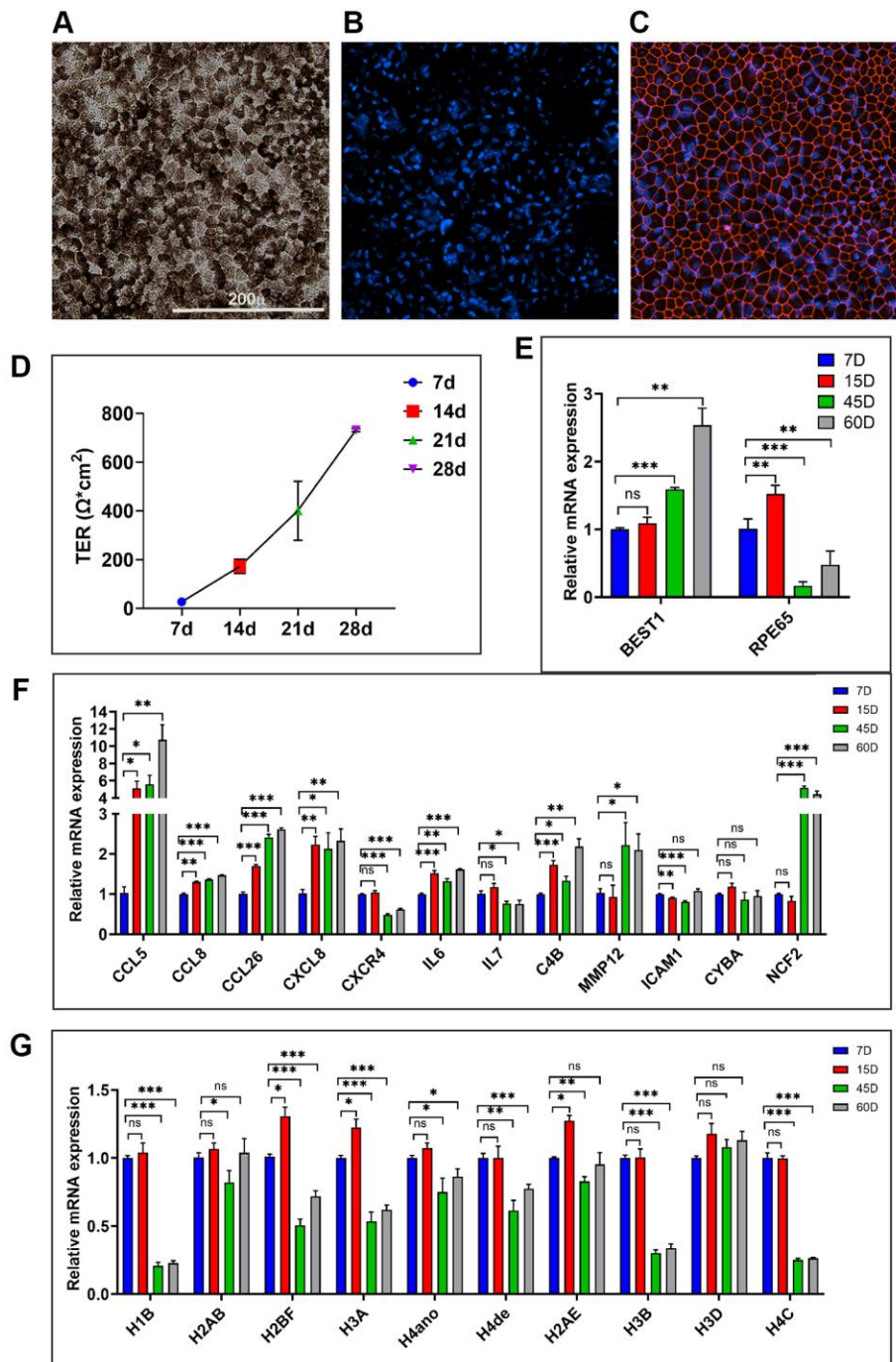


Figure 7. Evaluating the *in vitro* hRPE aging model. (A) Representative image of 21-day hRPE confluent cultures exhibit pigmentation and hexagonal cellular monolayers. (B, C) Representative immunofluorescence staining for the tight junction marker ZO-1 (Red) on day 21 and the nuclei are co-stained with Hoechst (Blue). (D) Time-dependent increase in TER from multiple transwells containing long-term primary hRPE cultures measured at 7/14/21 and 28 days. (E) Expression of RPE marker genes, *BEST1* and *RPE65* in the long-term hRPE cultures. (F, G) Relative mRNA expression levels of genes are significantly upregulated and downregulated in long-term hRPE cultures. Actin-B was used for normalization, and statistical analysis was performed using the unpaired *t*-test (**p* < 0.05, ***p* < 0.01, ****p* < 0.001, ns: nonsignificant). Data were presented as mean ± SEM.

immunofluorescent images of 21-day cultures stained positively for the tight junction protein, ZO-1, indicating continuous junctions between cells (Figure 7B, 7C). Weekly measurements of transepithelial resistance (TER) revealed a progressive increase, with hRPE cells ($n = 3$) developing a maximum resistance of $731.2 (\pm 6.6) \Omega \cdot \text{cm}^2$ at 28 days. Resistances ranging from $172.3 (\pm 28.8)$ to $731.2 (\pm 6.6) \Omega \cdot \text{cm}^2$, observed between days 14 and 21 in this long-term culture, surpassed the typical TER values of the human RPE monolayer ($150 \Omega \cdot \text{cm}^2$) *in vivo* [27] (Figure 7D). This suggests that the hRPE cells achieved functional polarization and tight junction formation. While the long-term cultures expressed RPE markers RPE65 and BEST1, the expression of these markers was altered with increasing culture time (Figure 7E).

As many previous studies [28, 29] have identified the 21-day timepoint as optimal for establishing long-term RPE cultures, we extended culturing hRPE cells to 45 and 60 days to obtain aged cells. To evaluate whether the long-term primary hRPE cultures can serve as a model for RPE aging, we used qPCR to assess a panel of proinflammatory, immune response, matrix remodeling, and oxidative stress-related genes from cultures of 7/15/45 and 60 days (Figure 7F). These genes were significantly altered with age in our *in vivo* transcriptomic data. Furthermore, a subset of these genes was also found to be significantly altered in the *in vitro* replicative model of hRPE aging, as reported in our recent study [30]. We examined the time-course expression trend of *CCL5*, *CCL8*, *CCL26*, *CXCL8*, *CXCR4*, *IL6*, *C4B*, *MMP12*, *ICAM1*, *CYBA*, and *NCF2* genes. In accordance with our *in vivo* aging RPE data, *CCL5*, *CCL8*, *CCL26*, *CXCL8*, *IL6*, *C4B*, *MMP12*, and *NCF2* genes exhibited a progressive increase in expression across the time course analysis (Figure 7F). These findings indicate the acquisition of an inflammatory and immunologically active phenotype, along with upregulation of redox stress response in chronologically aged *in vitro* hRPE cultures. While *CXCR4* showed a significant downregulation across different time points, *ICAM1* and *CYBA* showed no change in expression levels.

We analyzed histone expression levels in chronologically aged hRPE cells, building upon our recent demonstration of significant histone downregulation in aging mouse and human RPE *in vivo* [30]. A progressive depletion of various histone isoforms was observed at 15, 45, and 60 days (Figure 7G) compared to 7-day controls. Certain histone isoforms like *H1B*, *H2BF*, *H3A*, *H3B*, and *H4C* were substantially depleted with increasing culture time, unlike *H2AB* and *H3D*, which remain unchanged. Together, these findings highlight that chronological aging of RPE, both *in vivo*

and *in vitro*, is marked by the upregulation of inflammation genes and oxidative stress genes. Our model of long-term hRPE cultures recapitulated many validated cellular and molecular signatures of the aging RPE *in vivo*.

DISCUSSION

The primary objective of the current study was to elucidate the gene expression changes occurring during the natural aging process of the RPE by comparing transcriptome profiles between young and aged mice. Given the central role of RPE in age-related pathologies like AMD, understanding the precise molecular changes that take place in the RPE during aging is imperative [31]. Our analysis revealed divergence in the transcriptomes of RPE tissues from young and aged mice, as evidenced by the PCA. Notably, chronological aging emerged as the primary source of variation in the entire dataset, predominantly attributed to PC1. Functional enrichment of the genes driving PC1 identified immune and inflammation-related genes as the principal drivers of age-related alterations in gene expression. This observation aligns with previous research indicating the emergence of a low-grade inflammatory state known as the senescence-associated secretory phenotype (SASP) in aging mouse RPE [30].

In our study, a substantial number of protein-coding transcripts exhibited significant upregulation in the RPE of aging mice compared to their younger counterparts. This heightened transcriptional activity was reflected in the upregulation of numerous genes encoding immune regulators and proinflammatory factors across cellular locations, including the extracellular space, cell surface, membrane, and extracellular matrix. Similar patterns of increased immune and inflammatory responses have been noted in studies examining aging RPE in humans and non-human primates [7, 32]. Polarized RPE cells interact with the ECM-rich interphotoreceptor matrix and outer segments of photoreceptor cells at the apical surface and with Bruch's membrane at the basal surface. While the normal RPE actively participates in the ECM synthesis, with advancing age, the ECM microenvironment undergoes substantial changes compromising RPE homeostasis and function [33]. This alteration leads to diminished cell adhesion, proliferation, and migration, as well as reduced phagocytosis of photoreceptor outer segments. Moreover, the evolving ECM landscape influences ECM-associated immune and inflammatory processes [34, 35]. Lastly, the identification of abundant long non-coding RNAs (lncRNAs) reveals another layer of complexity governing the transcriptomic milieu of RPE cells and warrants exploration in future investigations.

GO enrichment analysis of DE genes downregulated in aging revealed biological processes related to the regulation of visual processes, particularly at the RPE-photoreceptor interface. This emphasizes aging as a significant risk factor disrupting the homeostasis of the RPE-photoreceptor system. The RPE plays a crucial role in the visual cycle. Light absorption by rhodopsin in photoreceptors initiates phototransduction, converting 11-cis-retinal to all-trans-retinal (atRAL). This atRAL is then transported to RPE cells where it undergoes conversion back to 11-cis-retinal before being returned to photoreceptors to regenerate rhodopsin, thus completing the cycle [36]. Dysfunctions in the visual cycle result in the accumulation of atRAL, leading to the degeneration of both photoreceptor and RPE cells due to their intimate symbiotic relationship.

Over-representation analysis of DE genes identified functional pathways enriched in both young and aged mice RPE/choroid. The most enriched pathway observed in aged mice RPE/choroid was the cytokine-cytokine receptor pathway. Pathway mapping showed the upregulation of diverse groups of chemotactic cytokines and chemokines that belong to CC, CXC, C families and their receptors. Several members of the interleukins (IL), interferons (IFN), tumor necrosis factor (TNF), and Transforming Growth Factor (TGF) family upregulated in aging RPE were also mapped to the pathway (Supplementary Figure 1). Members of the cytokine family have been implicated in the recruitment of immune cells and activation of inflammatory pathways that ultimately contribute to RPE degeneration and AMD pathogenesis. Other pathways, such as osteoclast differentiation, complement activation, coagulation cascades, chemokine signaling, and hematopoietic cell lineage were also upregulated in aged RPE/choroid. Previous studies have reported some common genes involved in RPE reprogramming and osteoclast differentiation [37, 38]. The young RPE/choroid was most enriched in pathways involved in phototransduction and protein digestion and absorption.

The interaction network of the DE genes was used to derive the hub genes, which may be central to RPE aging pathways and could serve as potential biomarkers for the diagnosis and treatment of age-related retinal diseases. In our study, the 20 hub genes include the five subunits of the NADPH oxidase complex, which is directly involved in ROS production [39]. Physiologic ROS production in the RPE is involved in signal transduction cascades, and typically RPE oxidative stress is reduced by endogenous RPE antioxidants and antioxidant enzymes such as superoxide dismutase (SOD) and catalase and glutathione peroxidase (GPX) [40, 41]. With aging, these RPE defenses diminish, allowing heightened ROS production and apoptotic

damage [42–44]. Proinflammatory cytokines are known to stimulate increased ROS production through the NADPH oxidase complex in RPE cells [45]. The hub genes also include genes from the chemokine pathway and the complement pathway, all of which indicate the immunologically charged environment of the RPE. PPI network of genes downregulated in aged RPE mainly involved histones, genes involved in phototransduction, and neural networks. Downregulation of histones in the aged RPE was recently reported by our group and further validated here as a critical age-related feature in the STRING network [30].

In vitro cultures have been utilized as aging research models for various cell types, yet their application to RPE models remains largely unexplored [46, 47]. Utilizing *in vitro* models offers distinct advantages such as lower cost, reduced animal use, and improved efficiency in screening for signaling pathways and therapeutic targets. One of our study objectives was to assess long-term hRPE cultures as a model for studying aging by comparing cellular characteristics and transcriptomic profiling with *in vivo* models. Previous studies have identified a TER of approximately 200 $\Omega\cdot\text{cm}^2$ as a feature of fully differentiated RPE culture, closely reflecting the physiology of native RPE [48–52]. *In vitro* RPE cultures typically achieve full differentiation by day 21, with well-established cell-cell junctions. Although TER continues to increase beyond day 21, the rate of this increase tends to slow [53, 54]. The current findings demonstrate that our long-term hRPE cultures maintain morphology, pigmentation, and polarity (TER of 731.2 (± 6.6) $\Omega\cdot\text{cm}^2$ by day 28) even after extended culturing.

A notable gap in this field is the lack of studies investigating the global gene expression patterns of fetal hRPE to delineate the transition from maturation to aging; an important consideration when screening RPE cells for translational cell therapies. The monolayer culture system used in this study lacks interactions with the photoreceptor layer and the underlying Bruch's membrane, factors which could influence the growth and maturation trajectory of hRPE cells [55]. However, a comparison of age-related gene expression changes between long-term *in vitro* models and physiologically aged mouse RPE revealed significant overlap. These changes include upregulation of genes involved in pro-inflammatory responses, matrix remodeling, and oxidative stress, alongside downregulation of genes related to visual processes. We demonstrate that the transcriptional programs underlying hRPE aging *in vitro* recapitulate gene expression patterns of *in vivo* models. Thus, long-term hRPE cultures provide a valuable tool for evaluating the effects of chronological aging on cellular functions and high-throughput screening of potential therapeutic

targets. However, this study has limitations, including sample size ($n = 4$ per group) and the need for a more comprehensive transcriptome analysis to enhance the relevance of long-term *in vitro* models for aging research applications. To address this, our future work will focus on temporal transcriptome profiling at 1, 2, 4, and 6 months to gain a deeper understanding of the gene expression changes occurring with prolonged culturing of hRPE cells. While additional *in vitro* studies of mouse RPE cells would have been beneficial for comparison, technical challenges associated with long-term culturing of mouse RPE cells, as noted in previous studies, remain a significant barrier [56, 57].

Age-related alterations within RPE cells manifest as inflammation, immune activation, heightened oxidative stress, and diminished visual perception. Butler et al. [58] observed an upregulation of visual cycle genes in aging human donor RPE. However, our findings, align with previous microarray investigations in young and aged mouse RPE, delving into age-related alterations in gene expression [59, 60], and offers a more comprehensive analysis of the entire RPE/choroid transcriptome in young and aged mice. *In vitro* studies have shown that inflammatory cytokine treatment can downregulate genes critical for RPE function, including those involved in the visual cycle such as *CDH1*, *RPE65*, *RDH5*, *RDH10*, *TYR*, and *MERTK* [61]. This suggests that aging RPE, with elevated proinflammatory gene expression, experiences a decrease in visual cycle pathway gene expression in mouse RPE. These observations highlight species-specific transcriptional differences underlying age-related changes between humans and other model systems [26].

Leveraging RNA sequencing and bioinformatics tools provides a robust approach to uncover the molecular mechanisms underlying RPE aging. Data mining employing GO and KEGG pathway analysis tools reveals enriched genes linked to RPE aging. Through PPI visualization and analysis of hub genes using STRING and Cytoscape, we identified aging upregulated pathways and key nodes with significant influence on the network. In conclusion, our study delineates the gene signatures associated with pro-inflammatory responses, immune activation, and oxidative stress in RPE aging, laying the groundwork for therapeutic interventions aimed at delaying aging processes and targeting age-related retinal diseases.

MATERIALS AND METHODS

Animals

All mouse experiments complied with the guidelines established by the Association for Research in Vision

and Ophthalmology for the Use of Animals in Ophthalmic and Vision Research. Male and female wild-type C57BL/6J mice aged between 2 and 3 months were included in the young group ($n = 4$), while mice aged between 20 and 24 months were assigned to the aged group ($n = 4$). The mice were purchased from the Jackson Laboratory and housed under standard conditions ($23 \pm 1^\circ\text{C}$, 40–50% humidity, and ad libitum access to food and water). The Institutional Animal Care and Use Committee of the East Tennessee State University approved the research protocol.

Mouse RPE/choroid collection

RPE/choroid from young and aged mice were collected as described by Dubey et al. [30]. To harvest mouse RPE, isolated eyes were placed on a cold petri dish beneath a surgical microscope. The anterior sections of the eye were precisely excised and symmetrical radial cuts were made in a four-leaf pattern to carefully remove the neural retina from the mouse eyecup. The pigmented RPE/choroid layer was gently scraped from the sclera and was promptly transferred to TRIzol (Invitrogen 12183016, Carlsbad, CA, USA) for RNA isolation. The tissues were swiftly snap-frozen and preserved in liquid nitrogen if not used immediately.

RNA isolation

For RNA sequencing analysis, RPE/choroid tissue (2 eyes/sample) was collected from young and aged mice ($n = 4$; two males and two females per group). RNA extraction was performed from TRIzol according to the manufacturer's instructions. Following this, RNA purification and on-column genomic DNA digestion were carried out using the Pure Link RNA Micro Kit (Invitrogen 12183016, Carlsbad, CA, USA). The quality of RNA samples was evaluated using the Agilent 2100 Bioanalyzer system (Agilent, Santa Clara, CA, USA), ensuring a median concentration of 40 ng/ μl and RIN values >9 to facilitate library preparation.

Library preparation and sequencing

Library construction and sequencing on the Illumina NovaSeq X Plus platform were carried out at the Rush University Core Genomics Facility and the Roy J. Carver Biotechnology Center, University of Illinois, at Urbana-Champaign, respectively. The samples underwent a DNase treatment and clean-up using the Qiagen RNase-Free DNase Set (Catalog: 79254) paired with the Qiagen RNeasy[®] Mini QIAcube Kit (Catalog: 74116). A normalized total of about 200 ng went into the treatment/clean-up and was carried out per the manufacturer's instructions on the QIAcube Connect instrument. The samples were assessed for

quality post-treatment using High Sensitivity RNA ScreenTape Analysis by Agilent (catalog: 5067-5579 and 5067-5580) and the samples were normalized to 30 ng for library preparation. Samples underwent rRNA depletion as part of the library preparation using Revvity NEXTFLEX[®] RiboNaut rRNA Depletion Kit (catalog: NOVA-512963). Post depletion the Revvity NEXTFLEX[®] Rapid Directional RNA-Seq Automation Kit 2.0 (catalog: NOVA-5198-53) was used to finish the library preparation. Both processes were carried out on the Revvity Sciclone[®] G3 NGSx iQ[™] Workstation. Preliminary sequencing data was generated using the Illumina Miniseq[™] and used for normalization of libraries prior to final sequencing via Illumina's NovaSeq[™] X Plus Sequencing System. To prevent index switching, Unique Dual Indexes (UDIs) were used for barcoding the libraries. The library pool was further quantitated by qPCR on a BioRad CFX Connect Real-Time System (BioRad Laboratories, Inc. Hercules, CA, USA). The pooled barcoded libraries were multiplexed and loaded on one 10B lane on a NovaSeq X Plus for cluster formation and sequencing. The libraries were sequenced from both ends of the fragments for a total of 150 bp from each end. The fastq read files were generated and demultiplexed with the bcl2fastq v2.20 Conversion Software (Illumina, San Diego, CA, USA).

RNA-seq data mapping and analysis

Paired-end 150 bp raw reads were trimmed to eliminate Truseq adapters and bases from the 3' end with quality scores less than 20 using cutadapt (ver 4.4) [62]. Trimmed reads shorter than 40 bp were discarded. Subsequently, trimmed reads were aligned to the *Mus musculus* (house mouse) genome assembly GRCm39 (mm39) from Genome Reference Consortium (GCA_000001635.9 GCF_000001635.27) using STAR [63]. The expression level of ENSEMBL genes was quantified using FeatureCounts [64]. Differential expression statistics were computed using edgeR [65], using raw expression counts obtained from quantification. Normalized expression was computed as log₂ CPM (counts per million), including a TMM normalization and batch effect correction. All *p*-values were adjusted for multiple testing using the false discovery rate (FDR) correction of Benjamini and Hochberg. Principal component analysis of normalized read counts of the whole transcriptome dataset was conducted to identify the primary source of variation, using the "prcomp" function in the R statistical environment (R v.4.3.1). A volcano plot of DEGs was generated using the EnhancedVolcano R package. Hierarchical clustering and heat maps were constructed with log₂-transformed normalized read counts utilizing the heatmap.2 function in R.

Gene ontology and kyoto encyclopedia of genes and genomes (KEGG) enrichment analyses of DEGs

GO and KEGG pathway analyses were carried out using the web tool ShinyGo (ShinyGO 0.80) [66]. To functionally classify the DEGs, we identified over-represented GO terms in three categories, namely biological process, molecular function, and cellular component categories. Enriched GO terms were visualized as bar charts, with a significance threshold of FDR <0.05. Additionally, KEGG [67] pathway enrichment analysis was conducted with an FDR cutoff of 0.05 for significance and the Pathview [68] visualization tool was used to map the RNA-seq data.

STRING-PPI and hub gene analysis

The STRING (v12.0) [23] online tool was used for predicting the PPI of proteins encoded by the upregulated and downregulated DEGs. Subsequently, a PPI network was constructed using the STRING database, with a high confidence score of ≥ 0.9 as the cutoff criterion. The outcomes of the STRING analysis were further processed using the clusterMaker2 plugin of Cytoscape tool (v3.8.2) [69, 70]. The large PPI network was subclustered by employing the Markov clustering (MCL) algorithm to form biologically relevant tightly linked protein networks, with the default granularity parameter (inflation value) set to 4. Hub genes within the PPI network were identified using the maximal clique centrality (MCC) algorithm of the CytoHubba [24] plugin of Cytoscape tool. Wikipathways [71] were imported into Cytoscape using the Wikipathways app, and RNA-seq data were overlaid using the built-in IdMapper functionality.

qPCR

Total RNA was extracted from hRPE cells and mice RPE/choroid tissues as described previously [72] and cDNA was synthesized using the High Capacity cDNA Reverse Transcription Kit (Applied Biosystems 4368814, Lithuania) according to the manufacturer's instructions. The qPCR was performed as described previously [72] using the primer list in Supplementary Table 3. Briefly, 20 ng cDNA was amplified using the Power SYBR Green PCR Master Mix (Applied Biosystems 4368706, Lithuania) and StepOnePlus Real-Time PCR System (Applied Biosystems, Lithuania). Relative gene expression changes were calculated using either GAPDH or Actin as the reference gene. The fold change was calculated by determining the ratio of mRNA levels to control values using the Δ threshold cycle (Ct) method ($2^{-\Delta\Delta Ct}$).

Immunofluorescence

Frozen mouse eye sections were processed for immunofluorescence as described previously [30]. After initial fixing and permeabilization, sections were blocked for 1 hour in a solution containing 4% normal goat serum and 3% bovine serum albumin in 1X PBS. The sections were then incubated with primary antibodies overnight at 4°C, followed by incubation with fluorescently tagged secondary antibodies for 1 h at RT. Nuclei were counterstained with Hoechst (1:10,000; Invitrogen) for 5 minutes. Primary antibodies used included anti-Histone H1.0 antibody (1:250; Cat# ab125027, Abcam), anti-C4 b/d antibody (1:250; Cat# NB200-541, Novusbio), and Isotype controls. Images were captured at 40X magnification using a TCS SP8 confocal microscope (Leica).

Establishment of long-term hRPE cultures and trans-Epithelial electrical resistance (TER) measurement

For long-term cultures, primary fetal human RPE cells ($n = 3$ isolates; Lonza, H-RPE 00194987, Walkersville, MD, USA) were seeded on fibronectin (356008, Corning, Bedford, MA, USA) coated 12 mm-polyester (PET) transwell inserts with 0.4 mm pores in a 12-well plate (#3460, Costar, Kennebunk, ME, USA) with 1×10^5 cells per well. These cells were initially cultured in RPE culture medium (RPECM, alpha-MEM plus 1% N1 Supplement, 1% Glutamine-Penicillin-Streptomycin, 1% non-essential amino acids, 250 mg/L taurine, 20 mg/L hydrocortisone, 0.013 mg/L triiodo-thyronine) containing 10% FBS and maintained in a humidified atmosphere at 37°C with 5% CO₂ and 95% air. After two days, when cells attained confluency, the FBS in the RPE medium was reduced to 1%. TER of hRPE cells was measured weekly after seeding transwell inserts using the EVOM2 Epithelial Volt-Ohm Meter (World Precision Instruments, Sarasota, FL, USA). In each plate, one coated insert without cells was measured as blank, and the final resistance was calculated by multiplication of net resistance (Total – blank, Ω) with effective membrane area (cm²).

ZO-1 immunostaining

Long-term human RPE cultures were fixed with 4% paraformaldehyde for 15 minutes and then permeabilized in PBS with 0.25% Triton X-100 for 15 min at room temperature. Cells were then blocked in PBS with 4% normal goat serum and 3% bovine serum albumin for 1 h followed by incubation with anti-ZO-1 primary antibody (1:200; Cat# 40-2200, Invitrogen, Rockford, IL, USA) in blocking buffer overnight at

4°C. After three serial PBS washes, cells were labeled with goat anti-rabbit secondary antibodies conjugated with Alexa Fluor 488 (1:1000; Cat# A11070, Invitrogen, Eugene, OR) for 1 h and then co-stained with Hoechst 33342 (1:10000; Cat# H3570, Invitrogen, Eugene, OR, USA) for 5 min. Fluorescent and bright-field images were acquired with confocal fluorescent microscopy (TCS SP8, Leica, Wetzlar, Germany).

Statistical analysis

GraphPad Prism (GraphPad Software, La Jolla, CA, USA) was used for routine statistical analysis. The results are presented as mean \pm standard error of the mean (SEM) or mean \pm standard deviation (SD). The significance levels were depicted as follows: * $p < 0.05$; ** $p < 0.01$; *** $p < 0.001$. Group comparisons were performed using a non-parametric unpaired t -test.

Data availability

Raw RNA-seq data from this manuscript were deposited to the GEO database under accession code GSE263427.

Abbreviations

RPE: Retinal pigment epithelium; AMD: Age-related macular degeneration; ROS: Reactive oxygen species; PCA: Principal component analysis; GO: Gene ontology; DEG: Differentially expressed genes; ECM: Extracellular matrix; PPI: Protein-protein interaction; TER: Trans-Epithelial Electrical Resistance.

AUTHOR CONTRIBUTIONS

SKD, RD, and MEK designed research; SKD, RD, KJ, and AGH performed research; SKD, RD, KJ, AGH, and MEK analyzed data; SKD, RD, and MEK provided edits of the paper; SKD, RD, and MEK wrote the paper.

ACKNOWLEDGMENTS

Library preparation, pooling, and sequencing were performed at the Genomics and Microbiome Core Facility (GMCF) at Rush University. Bioinformatics analysis and downstream processing were performed at the Rush Research Bioinformatics Core (RRBC) at Rush University.

CONFLICTS OF INTEREST

The authors declare no conflicts of interest related to this study.

ETHICAL STATEMENT

All mouse experiments were conducted in compliance with the guidelines established by the Association for Research in Vision and Ophthalmology for the Use of Animals in Ophthalmic and Vision Research. The Institutional Animal Care and Use Committee of the East Tennessee State University approved the research protocol (P210601). Studies utilizing primary human cells or tissues followed the guidelines of the Declaration of Helsinki and were exempt from IRB approval.

FUNDING

This work was supported by the grants from NIH R01EY028206 (Mark E. Kleinman), NIH K08EY021757 (Mark E. Kleinman), NIH R01EY036138 (Mark E. Kleinman), BrightFocus AMD Research Award (Mark E. Kleinman), American Federation for Aging Research (Mark E. Kleinman), and International Retinal Research Foundation (Sushil K. Dubey).

REFERENCES

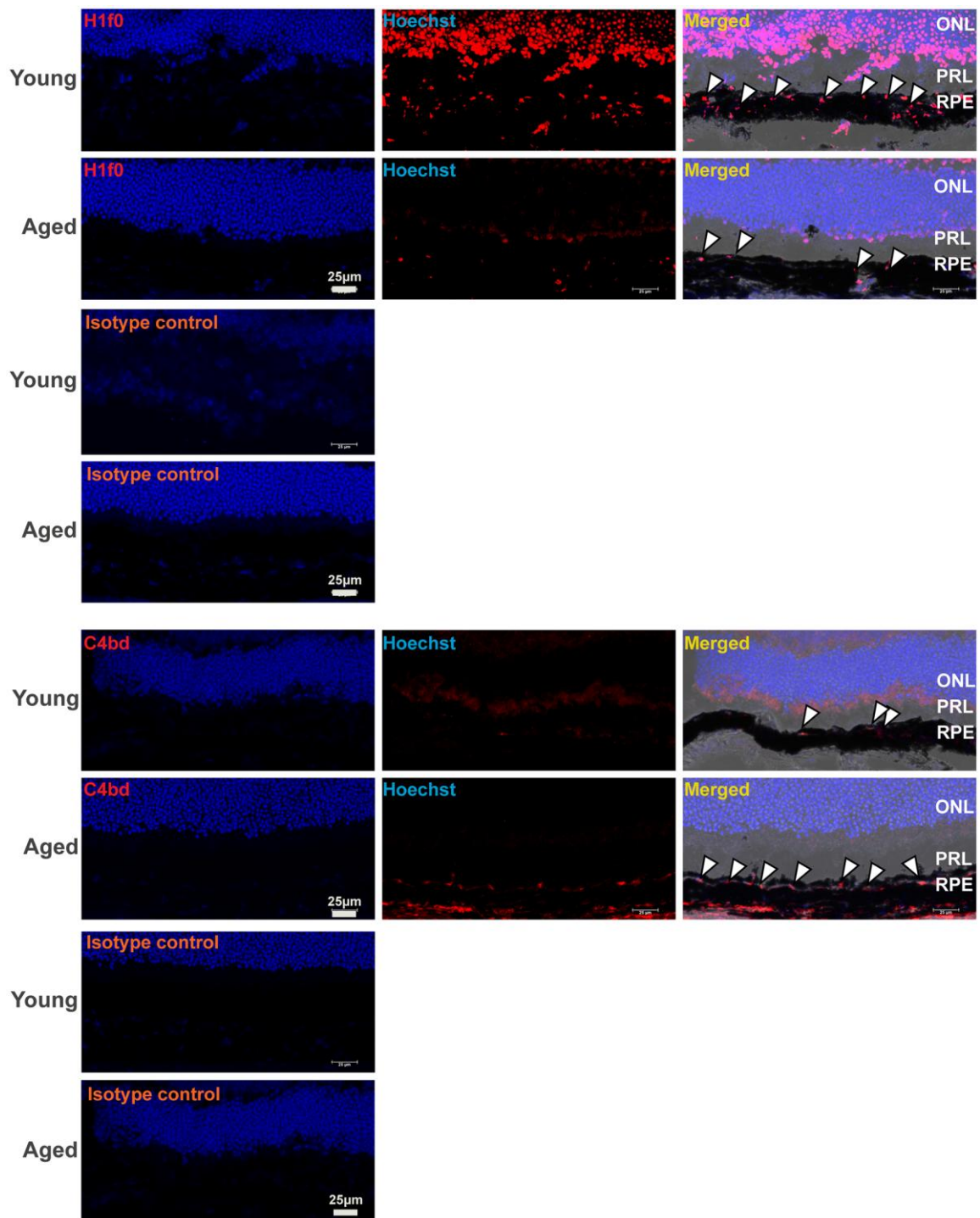
1. Rizzolo LJ. Polarity and the development of the outer blood-retinal barrier. *Histol Histopathol.* 1997; 12:1057–67. PMID:[9302567](https://pubmed.ncbi.nlm.nih.gov/9302567/)
2. Bok D. The retinal pigment epithelium: a versatile partner in vision. *J Cell Sci Suppl.* 1993; 17:189–95. <https://doi.org/10.1242/jcs.1993.supplement.17.27> PMID:[8144697](https://pubmed.ncbi.nlm.nih.gov/8144697/)
3. Wald G, Brown PK. Synthesis and bleaching of rhodopsin. *Nature.* 1956; 177:174–6. <https://doi.org/10.1038/177174a0> PMID:[13297008](https://pubmed.ncbi.nlm.nih.gov/13297008/)
4. Baehr W, Wu SM, Bird AC, Palczewski K. The retinoid cycle and retina disease. *Vision Res.* 2003; 43:2957–8. <https://doi.org/10.1016/j.visres.2003.10.001> PMID:[14611932](https://pubmed.ncbi.nlm.nih.gov/14611932/)
5. Wimmers S, Karl MO, Strauss O. Ion channels in the RPE. *Prog Retin Eye Res.* 2007; 26:263–301. <https://doi.org/10.1016/j.preteyeres.2006.12.002> PMID:[17258931](https://pubmed.ncbi.nlm.nih.gov/17258931/)
6. Young RW, Bok D. Participation of the retinal pigment epithelium in the rod outer segment renewal process. *J Cell Biol.* 1969; 42:392–403. <https://doi.org/10.1083/jcb.42.2.392> PMID:[5792328](https://pubmed.ncbi.nlm.nih.gov/5792328/)
7. Wang S, Zheng Y, Li Q, He X, Ren R, Zhang W, Song M, Hu H, Liu F, Sun G, Sun S, Liu Z, Yu Y, et al. Deciphering primate retinal aging at single-cell resolution. *Protein Cell.* 2021; 12:889–98. <https://doi.org/10.1007/s13238-020-00791-x> PMID:[33051815](https://pubmed.ncbi.nlm.nih.gov/33051815/)
8. Burton MJ, Ramke J, Marques AP, Bourne RRA, Congdon N, Jones I, Ah Tong BAM, Arunga S, Bachani D, Bascaran C, Bastawrous A, Blanchet K, Braithwaite T, et al. The Lancet Global Health Commission on Global Eye Health: vision beyond 2020. *Lancet Glob Health.* 2021; 9:e489–551. [https://doi.org/10.1016/S2214-109X\(20\)30488-5](https://doi.org/10.1016/S2214-109X(20)30488-5) PMID:[33607016](https://pubmed.ncbi.nlm.nih.gov/33607016/)
9. Rein DB, Wittenborn JS, Burke-Conte Z, Gulia R, Robalik T, Ehrlich JR, Lundeen EA, Flaxman AD. Prevalence of Age-Related Macular Degeneration in the US in 2019. *JAMA Ophthalmol.* 2022; 140:1202–8. <https://doi.org/10.1001/jamaophthalmol.2022.4401> PMID:[36326752](https://pubmed.ncbi.nlm.nih.gov/36326752/)
10. Guymer RH, Campbell TG. Age-related macular degeneration. *Lancet.* 2023; 401:1459–72. [https://doi.org/10.1016/S0140-6736\(22\)02609-5](https://doi.org/10.1016/S0140-6736(22)02609-5) PMID:[36996856](https://pubmed.ncbi.nlm.nih.gov/36996856/)
11. Kozlowski MR. RPE cell senescence: a key contributor to age-related macular degeneration. *Med Hypotheses.* 2012; 78:505–10. <https://doi.org/10.1016/j.mehy.2012.01.018> PMID:[22296808](https://pubmed.ncbi.nlm.nih.gov/22296808/)
12. Anderson DH, Mullins RF, Hageman GS, Johnson LV. A role for local inflammation in the formation of drusen in the aging eye. *Am J Ophthalmol.* 2002; 134:411–31. [https://doi.org/10.1016/s0002-9394\(02\)01624-0](https://doi.org/10.1016/s0002-9394(02)01624-0) PMID:[12208254](https://pubmed.ncbi.nlm.nih.gov/12208254/)
13. Lin H, Xu H, Liang FQ, Liang H, Gupta P, Havey AN, Boulton ME, Godley BF. Mitochondrial DNA damage and repair in RPE associated with aging and age-related macular degeneration. *Invest Ophthalmol Vis Sci.* 2011; 52:3521–9. <https://doi.org/10.1167/iovs.10-6163> PMID:[21273542](https://pubmed.ncbi.nlm.nih.gov/21273542/)
14. Delori FC, Goger DG, Dorey CK. Age-related accumulation and spatial distribution of lipofuscin in RPE of normal subjects. *Invest Ophthalmol Vis Sci.* 2001; 42:1855–66. PMID:[11431454](https://pubmed.ncbi.nlm.nih.gov/11431454/)
15. Crabb JW, Miyagi M, Gu X, Shadrach K, West KA, Sakaguchi H, Kamei M, Hasan A, Yan L, Rayborn ME, Salomon RG, Hollyfield JG. Drusen proteome analysis: an approach to the etiology of age-related macular degeneration. *Proc Natl Acad Sci U S A.* 2002; 99:14682–7. <https://doi.org/10.1073/pnas.222551899> PMID:[12391305](https://pubmed.ncbi.nlm.nih.gov/12391305/)
16. Russell SR, Mullins RF, Schneider BL, Hageman GS.

- Location, substructure, and composition of basal laminar drusen compared with drusen associated with aging and age-related macular degeneration. *Am J Ophthalmol*. 2000; 129:205–14.
[https://doi.org/10.1016/s0002-9394\(99\)00345-1](https://doi.org/10.1016/s0002-9394(99)00345-1)
PMID:10682974
17. Dieguez HH, Romeo HE, Alaimo A, González Fleitas MF, Aranda ML, Rosenstein RE, Dorfman D. Oxidative stress damage circumscribed to the central temporal retinal pigment epithelium in early experimental non-exudative age-related macular degeneration. *Free Radic Biol Med*. 2019; 131:72–80.
<https://doi.org/10.1016/j.freeradbiomed.2018.11.035>
PMID:30502459
 18. Liang FQ, Godley BF. Oxidative stress-induced mitochondrial DNA damage in human retinal pigment epithelial cells: a possible mechanism for RPE aging and age-related macular degeneration. *Exp Eye Res*. 2003; 76:397–403.
[https://doi.org/10.1016/s0014-4835\(03\)00023-x](https://doi.org/10.1016/s0014-4835(03)00023-x)
PMID:12634104
 19. Boyer DS, Schmidt-Erfurth U, van Lookeren Campagne M, Henry EC, Brittain C. The pathophysiology of geographic atrophy secondary to age-related macular degeneration and the complement pathway as a therapeutic target. *Retina*. 2017; 37:819–35.
<https://doi.org/10.1097/IAE.0000000000001392>
PMID:27902638
 20. Desai D, Dugel PU. Complement cascade inhibition in geographic atrophy: a review. *Eye (Lond)*. 2022; 36:294–302.
<https://doi.org/10.1038/s41433-021-01765-x>
PMID:34999723
 21. Holtkamp GM, Kijlstra A, Peek R, de Vos AF. Retinal pigment epithelium-immune system interactions: cytokine production and cytokine-induced changes. *Prog Retin Eye Res*. 2001; 20:29–48.
[https://doi.org/10.1016/s1350-9462\(00\)00017-3](https://doi.org/10.1016/s1350-9462(00)00017-3)
PMID:11070367
 22. Eamegdool SS, Sitiwin EI, Cioanca AV, Madigan MC. Extracellular matrix and oxidative stress regulate human retinal pigment epithelium growth. *Free Radic Biol Med*. 2020; 146:357–71.
<https://doi.org/10.1016/j.freeradbiomed.2019.11.018>
PMID:31751761
 23. Szklarczyk D, Gable AL, Lyon D, Junge A, Wyder S, Huerta-Cepas J, Simonovic M, Doncheva NT, Morris JH, Bork P, Jensen LJ, Mering CV. STRING v11: protein-protein association networks with increased coverage, supporting functional discovery in genome-wide experimental datasets. *Nucleic Acids Res*. 2019; 47:D607–13.
<https://doi.org/10.1093/nar/gky1131>
PMID:30476243
 24. Chin CH, Chen SH, Wu HH, Ho CW, Ko MT, Lin CY. cytoHubba: identifying hub objects and sub-networks from complex interactome. *BMC Syst Biol*. 2014 (Suppl 4); 8:S11.
<https://doi.org/10.1186/1752-0509-8-S4-S11>
PMID:25521941
 25. Kelder T, van Iersel MP, Hanspers K, Kutmon M, Conklin BR, Evelo CT, Pico AR. WikiPathways: building research communities on biological pathways. *Nucleic Acids Res*. 2012; 40:D1301–7.
<https://doi.org/10.1093/nar/gkr1074>
PMID:22096230
 26. Bennis A, Gorgels TG, Ten Brink JB, van der Spek PJ, Bossers K, Heine VM, Bergen AA. Comparison of Mouse and Human Retinal Pigment Epithelium Gene Expression Profiles: Potential Implications for Age-Related Macular Degeneration. *PLoS One*. 2015; 10:e0141597.
<https://doi.org/10.1371/journal.pone.0141597>
PMID:26517551
 27. Quinn RH, Miller SS. Ion transport mechanisms in native human retinal pigment epithelium. *Invest Ophthalmol Vis Sci*. 1992; 33:3513–27.
PMID:1334477
 28. Sugino IK, Rapista A, Sun Q, Wang J, Nunes CF, Cheewatrakoolpong N, Zarbin MA. A method to enhance cell survival on Bruch's membrane in eyes affected by age and age-related macular degeneration. *Invest Ophthalmol Vis Sci*. 2011; 52:9598–609.
<https://doi.org/10.1167/iovs.11-8400>
PMID:22039244
 29. Sugino IK, Sun Q, Wang J, Nunes CF, Cheewatrakoolpong N, Rapista A, Johnson AC, Malcuit C, Klimanskaya I, Lanza R, Zarbin MA. Comparison of FRPE and human embryonic stem cell-derived RPE behavior on aged human Bruch's membrane. *Invest Ophthalmol Vis Sci*. 2011; 52:4979–97.
<https://doi.org/10.1167/iovs.10-5386>
PMID:21460262
 30. Dubey SK, Dubey R, Prajapati SC, Jung K, Mohan K, Liu X, Roney J, Tian W, Abney J, Giarmarco MM, Hernandez AG, Liu J, Kleinman ME. Histone deficiency and hypoacetylation in the aging retinal pigment epithelium. *Aging Cell*. 2024; 23:e14108.
<https://doi.org/10.1111/acer.14108>
PMID:38408164

31. Boulton M, Dayhaw-Barker P. The role of the retinal pigment epithelium: topographical variation and ageing changes. *Eye (Lond)*. 2001; 15:384–9. <https://doi.org/10.1038/eye.2001.141> PMID:[11450762](https://pubmed.ncbi.nlm.nih.gov/11450762/)
32. Lee KS, Lin S, Copland DA, Dick AD, Liu J. Cellular senescence in the aging retina and developments of senotherapies for age-related macular degeneration. *J Neuroinflammation*. 2021; 18:32. <https://doi.org/10.1186/s12974-021-02088-0> PMID:[33482879](https://pubmed.ncbi.nlm.nih.gov/33482879/)
33. Fernandez-Godino R, Bujakowska KM, Pierce EA. Changes in extracellular matrix cause RPE cells to make basal deposits and activate the alternative complement pathway. *Hum Mol Genet*. 2018; 27:147–59. <https://doi.org/10.1093/hmg/ddx392> PMID:[29095988](https://pubmed.ncbi.nlm.nih.gov/29095988/)
34. Biasella F, Plössl K, Baird PN, Weber BHF. The extracellular microenvironment in immune dysregulation and inflammation in retinal disorders. *Front Immunol*. 2023; 14:1147037. <https://doi.org/10.3389/fimmu.2023.1147037> PMID:[36936905](https://pubmed.ncbi.nlm.nih.gov/36936905/)
35. Nita M, Strzałka-Mrozik B, Grzybowski A, Mazurek U, Romaniuk W. Age-related macular degeneration and changes in the extracellular matrix. *Med Sci Monit*. 2014; 20:1003–16. <https://doi.org/10.12659/MSM.889887> PMID:[24938626](https://pubmed.ncbi.nlm.nih.gov/24938626/)
36. Strauss O. The retinal pigment epithelium in visual function. *Physiol Rev*. 2005; 85:845–81. <https://doi.org/10.1152/physrev.00021.2004> PMID:[15987797](https://pubmed.ncbi.nlm.nih.gov/15987797/)
37. Lueck K, Carr AF, Stampoulis D, Gerke V, Rescher U, Greenwood J, Moss SE. Regulation of retinal pigment epithelial cell phenotype by Annexin A8. *Sci Rep*. 2017; 7:4638. <https://doi.org/10.1038/s41598-017-03493-3> PMID:[28680125](https://pubmed.ncbi.nlm.nih.gov/28680125/)
38. Takeda K, Yasumoto Ki, Kawaguchi N, Udono T, Watanabe Ki, Saito H, Takahashi K, Noda M, Shibahara S. Mitf-D, a newly identified isoform, expressed in the retinal pigment epithelium and monocyte-lineage cells affected by Mitf mutations. *Biochim Biophys Acta*. 2002; 1574:15–23. [https://doi.org/10.1016/s0167-4781\(01\)00339-6](https://doi.org/10.1016/s0167-4781(01)00339-6) PMID:[11955610](https://pubmed.ncbi.nlm.nih.gov/11955610/)
39. Tarafdar A, Pula G. The Role of NADPH Oxidases and Oxidative Stress in Neurodegenerative Disorders. *Int J Mol Sci*. 2018; 19:3824. <https://doi.org/10.3390/ijms19123824> PMID:[30513656](https://pubmed.ncbi.nlm.nih.gov/30513656/)
40. Newsome DA, Dobard EP, Liles MR, Oliver PD. Human retinal pigment epithelium contains two distinct species of superoxide dismutase. *Invest Ophthalmol Vis Sci*. 1990; 31:2508–13. PMID:[2265990](https://pubmed.ncbi.nlm.nih.gov/2265990/)
41. Tate DJ Jr, Newsome DA, Oliver PD. Metallothionein shows an age-related decrease in human macular retinal pigment epithelium. *Invest Ophthalmol Vis Sci*. 1993; 34:2348–51. PMID:[8505216](https://pubmed.ncbi.nlm.nih.gov/8505216/)
42. Samiec PS, Drews-Botsch C, Flagg EW, Kurtz JC, Sternberg P Jr, Reed RL, Jones DP. Glutathione in human plasma: decline in association with aging, age-related macular degeneration, and diabetes. *Free Radic Biol Med*. 1998; 24:699–704. [https://doi.org/10.1016/s0891-5849\(97\)00286-4](https://doi.org/10.1016/s0891-5849(97)00286-4) PMID:[9586798](https://pubmed.ncbi.nlm.nih.gov/9586798/)
43. Liles MR, Newsome DA, Oliver PD. Antioxidant enzymes in the aging human retinal pigment epithelium. *Arch Ophthalmol*. 1991; 109:1285–8. <https://doi.org/10.1001/archophth.1991.01080090111033> PMID:[1929958](https://pubmed.ncbi.nlm.nih.gov/1929958/)
44. Ballinger SW, Van Houten B, Jin GF, Conklin CA, Godley BF. Hydrogen peroxide causes significant mitochondrial DNA damage in human RPE cells. *Exp Eye Res*. 1999; 68:765–72. <https://doi.org/10.1006/exer.1998.0661> PMID:[10375440](https://pubmed.ncbi.nlm.nih.gov/10375440/)
45. Yang D, Elnor SG, Bian ZM, Till GO, Petty HR, Elnor VM. Pro-inflammatory cytokines increase reactive oxygen species through mitochondria and NADPH oxidase in cultured RPE cells. *Exp Eye Res*. 2007; 85:462–72. <https://doi.org/10.1016/j.exer.2007.06.013> PMID:[17765224](https://pubmed.ncbi.nlm.nih.gov/17765224/)
46. Rorteau J, Chevalier FP, Bonnet S, Barthélemy T, Lopez-Gaydon A, Martin LS, Bechetoille N, Lamartine J. Maintenance of Chronological Aging Features in Culture of Normal Human Dermal Fibroblasts from Old Donors. *Cells*. 2022; 11:858. <https://doi.org/10.3390/cells11050858> PMID:[35269480](https://pubmed.ncbi.nlm.nih.gov/35269480/)
47. Bigagli E, Luceri C, Scartabelli T, Dolara P, Casamenti F, Pellegrini-Giampietro DE, Giovannelli L. Long-term Neuroglial Cocultures as a Brain Aging Model: Hallmarks of Senescence, MicroRNA Expression Profiles, and Comparison With In Vivo Models. *J Gerontol A Biol Sci Med Sci*. 2016; 71:50–60. <https://doi.org/10.1093/gerona/glu231> PMID:[25568096](https://pubmed.ncbi.nlm.nih.gov/25568096/)
48. Hu J, Bok D. A cell culture medium that supports the differentiation of human retinal pigment epithelium

- into functionally polarized monolayers. *Mol Vis*. 2001; 7:14–9.
PMID:[11182021](https://pubmed.ncbi.nlm.nih.gov/11182021/)
49. Gallemore RP, Steinberg RH. Light-evoked modulation of basolateral membrane Cl⁻ conductance in chick retinal pigment epithelium: the light peak and fast oscillation. *J Neurophysiol*. 1993; 70:1669–80.
<https://doi.org/10.1152/jn.1993.70.4.1669>
PMID:[8283222](https://pubmed.ncbi.nlm.nih.gov/8283222/)
50. Maminishkis A, Chen S, Jalickee S, Banzon T, Shi G, Wang FE, Ehalt T, Hammer JA, Miller SS. Confluent monolayers of cultured human fetal retinal pigment epithelium exhibit morphology and physiology of native tissue. *Invest Ophthalmol Vis Sci*. 2006; 47:3612–24.
<https://doi.org/10.1167/iovs.05-1622>
PMID:[16877436](https://pubmed.ncbi.nlm.nih.gov/16877436/)
51. Sonoda S, Spee C, Barron E, Ryan SJ, Kannan R, Hinton DR. A protocol for the culture and differentiation of highly polarized human retinal pigment epithelial cells. *Nat Protoc*. 2009; 4:662–73.
<https://doi.org/10.1038/nprot.2009.33>
PMID:[19373231](https://pubmed.ncbi.nlm.nih.gov/19373231/)
52. Hazim RA, Karumbayaram S, Jiang M, Dimashkie A, Lopes VS, Li D, Burgess BL, Vijayaraj P, Alva-Ornelas JA, Zack JA, Kohn DB, Gomperts BN, Pyle AD, et al. Correction to: Differentiation of RPE cells from integration-free iPS cells and their cell biological characterization. *Stem Cell Res Ther*. 2019; 10:52.
<https://doi.org/10.1186/s13287-019-1147-7>
PMID:[30755264](https://pubmed.ncbi.nlm.nih.gov/30755264/)
53. Stanzel BV, Liu Z, Somboonthanakij S, Wongsawad W, Brinken R, Eter N, Corneo B, Holz FG, Temple S, Stern JH, Blenkinsop TA. Human RPE stem cells grown into polarized RPE monolayers on a polyester matrix are maintained after grafting into rabbit subretinal space. *Stem Cell Reports*. 2014; 2:64–77.
<https://doi.org/10.1016/j.stemcr.2013.11.005>
PMID:[24511471](https://pubmed.ncbi.nlm.nih.gov/24511471/)
54. Ablonczy Z, Dahrouj M, Tang PH, Liu Y, Sambamurti K, Marmorstein AD, Crosson CE. Human retinal pigment epithelium cells as functional models for the RPE in vivo. *Invest Ophthalmol Vis Sci*. 2011; 52:8614–20.
<https://doi.org/10.1167/iovs.11-8021>
PMID:[21960553](https://pubmed.ncbi.nlm.nih.gov/21960553/)
55. Sun R, Peng S, Chen X, Zhang H, Rizzolo LJ. Diffusible retinal secretions regulate the expression of tight junctions and other diverse functions of the retinal pigment epithelium. *Mol Vis*. 2008; 14:2237–62.
PMID:[19057659](https://pubmed.ncbi.nlm.nih.gov/19057659/)
56. Fernandez-Godino R, Garland DL, Pierce EA. Isolation, culture and characterization of primary mouse RPE cells. *Nat Protoc*. 2016; 11:1206–18.
<https://doi.org/10.1038/nprot.2016.065>
PMID:[27281648](https://pubmed.ncbi.nlm.nih.gov/27281648/)
57. Tomaszewski R, Rajpurohit P, Cheng M, Tawfik A. Isolation of Primary Mouse Retinal Pigmented Epithelium Cells. *J Vis Exp*. 2022; 10.3791/63543.
<https://doi.org/10.3791/63543>
PMID:[36408987](https://pubmed.ncbi.nlm.nih.gov/36408987/)
58. Butler JM, Supharattanasitthi W, Yang YC, Paraoan L. RNA-seq analysis of ageing human retinal pigment epithelium: Unexpected up-regulation of visual cycle gene transcription. *J Cell Mol Med*. 2021; 25:5572–85.
<https://doi.org/10.1111/jcmm.16569>
PMID:[33934486](https://pubmed.ncbi.nlm.nih.gov/33934486/)
59. Chen H, Liu B, Lukas TJ, Neufeld AH. The aged retinal pigment epithelium/choroid: a potential substratum for the pathogenesis of age-related macular degeneration. *PLoS One*. 2008; 3:e2339.
<https://doi.org/10.1371/journal.pone.0002339>
PMID:[18523633](https://pubmed.ncbi.nlm.nih.gov/18523633/)
60. Ida H, Boylan SA, Weigel AL, Hjelmeland LM. Age-related changes in the transcriptional profile of mouse RPE/choroid. *Physiol Genomics*. 2003; 15:258–62.
<https://doi.org/10.1152/physiolgenomics.00126.2003>
PMID:[14519767](https://pubmed.ncbi.nlm.nih.gov/14519767/)
61. Kutty RK, Samuel W, Boyce K, Cherukuri A, Duncan T, Jaworski C, Nagineni CN, Redmond TM. Proinflammatory cytokines decrease the expression of genes critical for RPE function. *Mol Vis*. 2016; 22:1156–68.
PMID:[27733811](https://pubmed.ncbi.nlm.nih.gov/27733811/)
62. Martin M. Cutadapt removes adapter sequences from high-throughput sequencing reads. 2011; 17:3.
<https://doi.org/10.14806/ej.17.1.200>
63. Dobin A, Davis CA, Schlesinger F, Drenkow J, Zaleski C, Jha S, Batut P, Chaisson M, Gingeras TR. STAR: ultrafast universal RNA-seq aligner. *Bioinformatics*. 2013; 29:15–21.
<https://doi.org/10.1093/bioinformatics/bts635>
PMID:[23104886](https://pubmed.ncbi.nlm.nih.gov/23104886/)
64. Liao Y, Smyth GK, Shi W. featureCounts: an efficient general purpose program for assigning sequence reads to genomic features. *Bioinformatics*. 2014; 30:923–30.
<https://doi.org/10.1093/bioinformatics/btt656>
PMID:[24227677](https://pubmed.ncbi.nlm.nih.gov/24227677/)
65. Robinson MD, McCarthy DJ, Smyth GK. edgeR: a Bioconductor package for differential expression analysis of digital gene expression data. *Bioinformatics*. 2010; 26:139–40.
<https://doi.org/10.1093/bioinformatics/btp616>
PMID:[19910308](https://pubmed.ncbi.nlm.nih.gov/19910308/)

66. Ge SX, Jung D, Yao R. ShinyGO: a graphical gene-set enrichment tool for animals and plants. *Bioinformatics*. 2020; 36:2628–9. <https://doi.org/10.1093/bioinformatics/btz931> PMID:31882993
67. Kanehisa M, Furumichi M, Sato Y, Ishiguro-Watanabe M, Tanabe M. KEGG: integrating viruses and cellular organisms. *Nucleic Acids Res*. 2021; 49:D545–51. <https://doi.org/10.1093/nar/gkaa970> PMID:33125081
68. Luo W, Brouwer C. Pathview: an R/Bioconductor package for pathway-based data integration and visualization. *Bioinformatics*. 2013; 29:1830–1. <https://doi.org/10.1093/bioinformatics/btt285> PMID:23740750
69. Shannon P, Markiel A, Ozier O, Baliga NS, Wang JT, Ramage D, Amin N, Schwikowski B, Ideker T. Cytoscape: a software environment for integrated models of biomolecular interaction networks. *Genome Res*. 2003; 13:2498–504. <https://doi.org/10.1101/gr.1239303> PMID:14597658
70. Utriainen M, Morris JH. clusterMaker2: a major update to clusterMaker, a multi-algorithm clustering app for Cytoscape. *BMC Bioinformatics*. 2023; 24:134. <https://doi.org/10.1186/s12859-023-05225-z> PMID:37020209
71. Agrawal A, Balci H, Hanspers K, Coort SL, Martens M, Slechter DN, Ehrhart F, Digles D, Waagmeester A, Wassink I, Abbassi-Daloui T, Lopes EN, Iyer A, et al. WikiPathways 2024: next generation pathway database. *Nucleic Acids Res*. 2024; 52:D679–89. <https://doi.org/10.1093/nar/gkad960> PMID:37941138
72. Mohan K, Dubey SK, Jung K, Dubey R, Wang QJ, Prajapati S, Roney J, Abney J, Kleinman ME. Long-Term Evaluation of Retinal Morphology and Function in Rosa26-Cas9 Knock-In Mice. *Int J Mol Sci*. 2023; 24:5186. <https://doi.org/10.3390/ijms24065186> PMID:36982266



Supplementary Figure 2. Representative fluorescence images of retinal cross-sections from young and aged mice illustrating the expression levels of H1f0 and C4b/d in the RPE layer. Staining for the H1f0 histone variant (red) was stronger in the RPE of young mice (indicated by white arrows) compared to aged mice. Nuclei are stained with Hoechst (blue) in both young and aged retinas. Merged images combining the red and blue channels with brightfield illustrate the localization of H1f0 in the RPE layer. Conversely, the RPE of aged mice showed more intense staining for the complement factor C4b/d (red, white arrows) compared to young mice. The isotype control panel displayed no immunostaining and served as a negative control. Abbreviations: GCL: ganglion cell layer; IPL: inner plexiform layer; INL: inner nuclear layer; OPL: outer plexiform layer; ONL: outer nuclear layer; PRL: photoreceptor layer; RPE: retinal pigment epithelium. Scale bar: 25 µm.

Supplementary Tables

Supplementary Table 1. List of top 100 PC1 loading genes and GO analysis of positive and negative loading genes.

PC1 loading genes		
Sl. No	PC1_positive genes	PC1_negative genes
1	Mfge8	Gm52669
2	Il7r	Adamtsl2
3	Mamdc2	Tgtp2
4	Serpina3n	4933429O19Rik
5	Anpep	Gabra4
6	Clec4d	Gm41620
7	Gpnmb	Alkal2
8	Cd68	Nxn12
9	Cdo1	Wdr72
10	Atf3	Adgrl3
11	Gm14461	Gm46454
12	Fabp5	Opn4
13	Orm1	Gm41056
14	Stra6l	Nipal2
15	Lyz2	Rho
16	Trem2	Gm39041
17	Slc7a11	Gm34159
18	Pira2	Gm44867
19	Fabp4	Ccdc85a
20	Cd300lb	Gm40780
21	Cxcr1	Gm534
22	Atp6v0d2	A730049H05Rik
23	Lgals3	Gm46129
24	Csf2rb	Gm52634
25	Mcoln2	Krt8
26	Capg	Pcare
27	Itgam	Prph2
28	Tm4sf19	Gm52689
29	Cd200r4	Tcim
30	Gm20056	H4c17
31	Acp5	Rcvrn
32	Ms4a6d	Loxl4
33	Il1rn	Enpp2
34	Timp1	LOC118567855
35	Csf2rb2	Opn1mw
36	Tyrobp	Ush2a
37	Itgax	Lrit2
38	Cd84	Gpr139
39	Mmp12	4921534H16Rik
40	Slc11a1	St6galnac3
41	Dio2	Hs6st3
42	Pik3r5	Gbp4
43	Adam8	Tbc1d21

44	Havcr2	Atp7b
45	Adra1a	Gm15737
46	Galnt6	H19
47	Itgb2	Gm36746
48	Lyz1	Angptl4
49	Wfdc17	Rtl1
50	Pirb	Ano2
51	Hmcn2	Rab37
52	Gdf3	Gm46553
53	Bcl2a1b	Gm48957
54	Apod	Cacna1h
55	Galnt15	Gm52128
56	Ctss	Cldn10
57	Mpeg1	Gm15609
58	Kynu	Mme
59	Bpifb1	Rxfp3
60	Sfrp4	Mest
61	Laptn5	Sostdc1
62	4930430E12Rik	Chad
63	Cd53	Cutal
64	Pisd-ps3	Rian
65	Clec7a	Cdh6
66	Creg2	Trim12a
67	Mmp3	Gm51910
68	Cd36	Col1a1
69	Npy	Nr4a1
70	C3	Peg3
71	Pira1	Gdpd2
72	Tlr13	Tmprss2
73	H2-M2	Gm41253
74	Bcan	Clnka
75	Olfrl11	Tmem72
76	Acpp	3110053B16Rik
77	Necab2	Gja1
78	Ptx4	Dab1
79	Ly9	Gvin3
80	Cd51	Gvin1
81	Ly75	Frem2
82	Lilrb4a	Gm33489
83	Prb1	Grik1
84	Igkc	LOC118568169
85	Lcn2	Gsg1l
86	Slc7a15	Adam7
87	Cybb	Gm33050
88	Slamf7	Gm42339
89	Lilr4b	Cd163
90	Glipr1	Gm40766
91	Jchain	Gm51909

92	Cma1	Matn4
93	Igha	Ifi213
94	Ighg2b	C430049B03Rik
95	Mmp13	Asic2
96	Tpsb2	Trhde
97	Mcpt4	Sox11
98	Gm2423	Ggt1
99	Serpine3	Dlk1
100	Erich5	Cilp2

PC1_positive loading genes GO

Category	Term ID	Term name	nGenes	Pathway genes	Enrichment FDR	Fold enrichment
GO:BP	GO:0006952	Defense response	37	1546	2.80E-16	5.8
GO:BP	GO:0006955	Immune response	33	1619	3.00E-12	5
GO:BP	GO:0002376	Immune system process	40	2544	4.30E-12	3.8
GO:BP	GO:0009607	Response to biotic stimulus	29	1439	1.70E-10	4.9
GO:BP	GO:0043207	Response to external biotic stimulus	28	1403	4.10E-10	4.9
GO:BP	GO:0051707	Response to other organism	28	1400	4.10E-10	4.9
GO:BP	GO:0098542	Defense response to other organism	24	1012	6.10E-10	5.8
GO:BP	GO:0006954	Inflammatory response	20	698	1.80E-09	7
GO:BP	GO:0044419	Biological process involved in interspecies interaction between organisms	28	1524	2.00E-09	4.5
GO:BP	GO:0006950	Response to stress	42	3637	7.40E-09	2.8

PC1_negative loading genes GO

Category	Term ID	Term name	nGenes	Pathway genes	Enrichment FDR	Fold enrichment
GO:BP	GO:0009583	Detection of light stimulus	7	52	3.30E-07	44.1
GO:BP	GO:0007601	Visual perception	9	155	6.60E-07	19
GO:BP	GO:0050953	Sensory perception of light stimulus	9	159	6.60E-07	18.6
GO:BP	GO:0007602	Phototransduction	5	30	1.20E-05	54.7
GO:BP	GO:0009581	Detection of external stimulus	7	128	3.20E-05	17.9
GO:BP	GO:0009582	Detection of abiotic stimulus	7	127	3.20E-05	18.1
GO:BP	GO:0009584	Detection of visible light	5	41	3.40E-05	40
GO:BP	GO:0018298	Protein-chromophore linkage	3	11	8.40E-04	89.4
GO:BP	GO:0009416	Response to light stimulus	8	318	9.40E-04	8.2
GO:BP	GO:0009628	Response to abiotic stimulus	14	1199	1.90E-03	3.8

Supplementary Table 2. GO analysis of upregulated and downregulated DE genes in aged mouse RPE/choroid.

Aging upregulated DE genes						
Category	Term ID	Term name	nGenes	Pathway genes	Enrichment FDR	Fold enrichment
GO:BP	GO:0006955	Immune response	200	1580	7.50E-63	3.9
GO:BP	GO:0002682	Reg. of immune system proc.	182	1430	6.10E-57	3.9
GO:BP	GO:0006954	Inflammatory response	123	739	3.00E-49	5.1
GO:BP	GO:0006952	Defense response	180	1642	1.00E-46	3.4
GO:BP	GO:0001775	Cell activation	140	1070	4.90E-44	4
GO:BP	GO:0002684	Positive reg. of immune system proc.	128	897	4.90E-44	4.4
GO:BP	GO:0050776	Reg. of immune response	118	812	4.00E-41	4.5
GO:BP	GO:0045321	Leukocyte activation	127	949	1.10E-40	4.1
GO:BP	GO:0002252	Immune effector proc.	98	629	2.80E-36	4.8
GO:BP	GO:0002443	Leukocyte mediated immunity	69	392	3.70E-28	5.4
GO:CC	GO:0005615	Extracellular space	162	1714	1.50E-33	2.9
GO:CC	GO:0009986	Cell surface	117	992	3.40E-32	3.6
GO:CC	GO:0098552	Side of membrane	84	676	4.00E-24	3.8
GO:CC	GO:0009897	External side of plasma membrane	67	466	1.20E-22	4.4
GO:CC	GO:0030312	External encapsulating structure	57	505	2.80E-14	3.5
GO:CC	GO:0031012	Extracellular matrix	57	503	2.80E-14	3.5
GO:CC	GO:0062023	Collagen-containing extracellular matrix	42	373	2.40E-10	3.5
GO:CC	GO:0045121	Membrane raft	43	408	1.00E-09	3.2
GO:CC	GO:0098857	Membrane microdomain	43	409	1.00E-09	3.2
GO:CC	GO:0001772	Immunological synapse	14	44	3.60E-09	9.7
GO:MF	GO:0005102	Signaling receptor binding	124	1561	1.00E-17	2.4
GO:MF	GO:0140375	Immune receptor activity	27	130	6.30E-12	6.4
GO:MF	GO:0004175	Endopeptidase activity	48	478	2.00E-09	3.1
GO:MF	GO:0008233	Peptidase activity	58	670	4.10E-09	2.7
GO:MF	GO:0004896	Cytokine receptor activity	19	95	4.40E-08	6.1
GO:MF	GO:0004252	Serine-type endopeptidase activity	26	202	4.70E-07	3.9
GO:MF	GO:0008236	Serine-type peptidase activity	26	217	1.90E-06	3.7
GO:MF	GO:0008009	Chemokine activity	12	45	1.90E-06	8.2
GO:MF	GO:0017171	Serine hydrolase activity	26	222	2.30E-06	3.6
GO:MF	GO:0019955	Cytokine binding	20	144	5.40E-06	4.3
Aging downregulated DE genes						
Category	Term ID	Term name	nGenes	Pathway genes	Enrichment FDR	Fold enrichment
GO:BP	GO:0007601	Visual perception	16	155	2.50E-11	14.9
GO:BP	GO:0050953	Sensory perception of light stimulus	16	159	2.50E-11	14.5
GO:BP	GO:0009583	Detection of light stimulus	10	52	1.90E-09	27.8
GO:BP	GO:0009584	Detection of visible light	8	41	2.20E-07	28.2
GO:BP	GO:0009581	Detection of external stimulus	11	128	6.20E-07	12.4
GO:BP	GO:0009582	Detection of abiotic stimulus	11	127	6.20E-07	12.5
GO:BP	GO:0007602	Phototransduction	6	30	1.90E-05	28.9
GO:BP	GO:0035458	Cellular response to interferon-beta	6	57	8.60E-04	15.2
GO:BP	GO:0035456	Response to interferon-beta	6	66	1.80E-03	13.1
GO:BP	GO:0009416	Response to light stimulus	11	318	3.50E-03	5
GO:CC	GO:0001750	Photoreceptor outer segment	8	88	1.80E-05	13.1
GO:CC	GO:0097730	Non-motile cilium	10	163	1.80E-05	8.9

GO:CC	GO:0097731	9+0 non-motile cilium	9	127	1.80E-05	10.2
GO:CC	GO:0097733	Photoreceptor cell cilium	9	114	1.80E-05	11.4
GO:CC	GO:0001917	Photoreceptor inner segment	6	73	6.70E-04	11.9
GO:CC	GO:0030312	External encapsulating structure	13	505	2.10E-03	3.7
GO:CC	GO:0031012	Extracellular matrix	13	503	2.10E-03	3.7
GO:CC	GO:0005929	Cilium	15	723	5.50E-03	3
GO:CC	GO:0005604	Basement membrane	5	115	4.00E-02	6.3
GO:CC	GO:0005615	Extracellular space	23	1714	4.40E-02	1.9
GO:MF	GO:0008020	G protein-coupled photoreceptor activity	3	10	3.20E-03	43.4
GO:MF	GO:0015267	Channel activity	13	483	3.20E-03	3.9
GO:MF	GO:0015318	Inorganic molecular entity transmembrane transporter activity	16	703	3.20E-03	3.3
GO:MF	GO:0022803	Passive transmembrane transporter activity	13	483	3.20E-03	3.9
GO:MF	GO:0022836	Gated channel activity	11	324	3.20E-03	4.9
GO:MF	GO:0005216	Ion channel activity	12	439	3.60E-03	4
GO:MF	GO:0015075	Ion transmembrane transporter activity	17	825	3.60E-03	3
GO:MF	GO:0009881	Photoreceptor activity	3	12	3.60E-03	36.1
GO:MF	GO:0005044	Scavenger receptor activity	4	46	1.20E-02	12.6
GO:MF	GO:0097110	Scaffold protein binding	5	82	1.20E-02	8.8

Supplementary Table 3. List of qPCR primers.

List of qPCR primers used in this study		
Primer name	Forward	Reverse
Mouse		
<i>Best1</i>	CATCAGCACCTCGGTCTACAAG	GACAAGTTGGCAAACCACACCC
<i>Bco2</i>	AACACGCGGTTTCATGTGGTGG	CCATCATCCTGGCAGCACAGAT
<i>C1qb</i>	CAACCAGGCACTCCAGGGATAA	CCAACTTTGCCTGGAGTCCCAG
<i>C1s1</i>	CAAAGCGATGGACAGTGGAGCA	CCAAACACACTATTCTCTGGCTC
<i>C3</i>	GGCCTTCTCTAACAGCCA	ATGCTGACCCTGAGGTCAA
<i>C4b</i>	GGAGAGTGAACCTGTAGACAG	CACTCGAACACGAGTTGGCTTG
<i>Cxcr1</i>	CCATTCCGTTCTGGTACAGTCTG	GTAGCAGACCAGCATAGTGAGC
<i>Cxcr4</i>	GACTGGCATAGTCGGCAATGGA	CAAAGAGGAGGTCAGCCACTGA
<i>Cyba</i>	GCTCATCTGTCTGCTGGAGTATC	CGGACGTAGTAATTCCTGGTGAG
<i>Cybb</i>	TGGCGATCTCAGCAAAAGGTGG	GTAAGTGTCCCACCTCCATCTTG
<i>Gria3</i>	GCAATGACAGCTCATCTCCGA	GCGCTCATTTCCTTCCAGTTGC
<i>Gnail</i>	CTCGGAAGAGGAGTGTAAGCAG	GCAAGCACGAAAAGTTGGCGAG
<i>Gnat1</i>	GCTTGTGGAAGGACTCGGGTAT	AACGCAACACGTCCTGCTCAGT
<i>Gpc3</i>	CTGTGCTGGAACGGACAAGAAC	GTCAATGATCTGGCTAACCACCG
<i>Grk4</i>	GATGGAGTCTCTGCTGTAAAGCA	CCTTTCACCACAGAGAACTGCC
<i>Gucy2f</i>	GGTGCTCCTTTCTGCATGATGG	GGCATACTCAGGAGAAACCACG
<i>H3c11</i>	TTCTAGTGTACTGAGATGGCTCGT	GTAGCGGTGAGGCTTCTTCA
<i>Hdac3</i>	GGCCAGAAGCACCAATGAGTTCTA	ACAATCATCAGGCCGTGAGAGTTTG
<i>Hdac8</i>	CAGAGGAACCCGCCAACAG	CGCAGATGCTGACATACTCGG
<i>H1f0</i>	GATGAGCCCAAAAGGTCGGT	CTTCTTGACAGGGGTGGCTT
<i>Napepld</i>	AATCACAGCGGCGTTCAGGTT	ACTCGTAAGCCAGCCTCTCTCA
<i>Ncf1</i>	GCTGACTACGAGAAGAGTTCGG	CCTCGCTTTGTCTTCATCTGGC
<i>Ncf2</i>	GCAGAAGAGCAGTTGGCATTGG	CTGCCCTCATTGGACGGAAC

<i>Ncf4</i>	CAAAGACCTGCTAGCGCTCATG	CCACATCCTCATCTGACAGCAG
<i>Rbp3</i>	CACCTCCCATTCTGCTGGACAA	ACACCACTGGTCAGGATGGCTA
<i>Rdh12</i>	GTGGTCATCACAGGTGCCAACA	GGAGTTCTTGGTATCTGCTCGG
<i>Rdh5</i>	CCATTGTGGAGCCTGGCTTCTT	ATGATGCGGCGCTGTACTCGAA
<i>Rdh8</i>	GGAGGACAAGTGGATGTGCTAG	CTTCATGCCTGGAAGCACAGCT
<i>Rpe65</i>	AAGGCTCCTCAGCCTGAAGTCA	GAGAACCTCAGGTTCCAGCCAT
<i>Tet1</i>	CCATTCTCACAAGGACATTCACA	GCAGGACGTGGAGTTGTTCA

Human

hCCL5	CCTGCTGCTTTGCCTACATTGC	ACACACTTGGCGGTTCTTTCCGG
hC4B	AGATGCGGTGTCCAAGGTTCTG	GTTGCCAGGTATTTCCAAGGTCC
hCCL26	GGGAGTGACATATCCAAGACCTG	CAGACTTTCTTGCCTCTTTTGGTA
hCCL8	TATCCAGAGGCTGGAGAGCTAC	TGGAATCCCTGACCCATCTCTC
hCXCR4	CTCCTCTTTGTCATCACGCTTCC	GGATGAGGACACTGCTGTAGAG
hCYBA	ACCAGGAATTACTATGTTCCGGC	TAGGTAGATGCCGCTCGCAATG
hNCF2	ACTACTGCCTGACTCTGTGGTG	CCTCCACTTGGCTGCCTTTCTT
hBEST1	TGCCAACCTGTCAATGAAGGCG	TCCAGTCGTAGGCATACAGGTG
hCXCL8	GAGAGTGATTGAGAGTGGACCAC	CACAACCCTCTGCACCCAGTTT
hH4A,N,O	GAGACAACATTCAGGGCATCAC	GAGGCCAGAGATCCGCTTAA
hH4C	AAGTTAAGAGTTGTTGTTTGTCTTCG	CCACCTTTGCCTCTACCAGA
hH4D,E	TGGGTGAGACTCCTCTTGCT	AAGACCCTTCCCGCCTTT
hHIST1H1B	CTAAGGAGCGCAATGGCCTTT	CTTCGGAGTCTTCTTCACTGC
hHIST1H2AE	CTACTCCGAACGAGTCGGG	GATGGTCACGCGACCTAGAAG
hHIST1H2BF	ACCTGCTAAGTCCGCTCCT	CTACGCTTGCCTTCTTACCA
hHIST1H3A	ACTGCTCGGAAAGTCTACTGGT	GCGCTGGAAAGGTAGTTTACGA
hHIST1H3B	ATGGCTCGTACTAAACAGACAGC	TTCCGAATCAGCAACTCGGTC
hHIST1H3D	CCATTCCAGCGTCTAGTCCG	TCTGAAAACGCAGATCAGTCTTG
hHIST2H2AB	CCATCTGCAACTAGCCGTGAG	CAGGCTTGTGACTCTCCGT
hICAM1	AGCGGCTGACGTGTGCAGTAAT	TCTGAGACCTCTGGCTTCGTCA
hIL6	ATCTGGATTCAATGAGGAGACTTG	GGAAGTGGATCAGGACTTTTGTACT
hMMP12	GATGCTGTCACTACCGTGGGAA	CAATGCCAGATGGCAAGGTTGG
hRPE65	TTTGGCACCTGTGCTTTCCAG	GTTGGTCTCTGTGCAAGCGTAG
